

# One-step $^{18}\text{F}$ -labeling and preclinical evaluation of prostate specific membrane antigen trifluoroborate probes for cancer imaging

Hsiou-Ting Kuo<sup>1,2,\*</sup>, Mathieu L. Lepage<sup>3,\*</sup>,<sup>†</sup>, Kuo-Shyan Lin<sup>1,2,†</sup>, Jinhe Pan<sup>1</sup>, Zhengxing Zhang<sup>1</sup>, Zhibo Liu<sup>3</sup>, Alla Pryyma<sup>3</sup>, Chengcheng Zhang<sup>1</sup>, Helen Merkens<sup>1,2</sup>, Aron Roxin<sup>1,3</sup>, David M. Perrin<sup>3,†</sup>, François Bénard<sup>1,2,†</sup>

<sup>1</sup>BC Cancer, 675 W 10th Ave, Vancouver, BC V5Z 1L3, Canada.

<sup>2</sup>Department of Radiology, University of British Columbia, 2775 Laurel Street, Vancouver, BC, V5Z 1M9

<sup>3</sup>Chemistry Department, University of British Columbia, 2036 Main Mall, Vancouver, BC V6T 1Z1, Canada.

\*Both authors contributed equally to this manuscript.

The first two authors are postdoctoral trainees.

<sup>†</sup>Three corresponding authors.

Addresses for correspondence:

Francois Benard, M.D.  
BC Cancer Research Centre  
675 West 10<sup>th</sup> Avenue  
Vancouver, BC, V5Z 1L3, Canada  
Telephone: 604-675-8206  
Email: [fbenard@bccrc.ca](mailto:fbenard@bccrc.ca)

David Perrin, Ph.D.  
Chemistry Department  
2036 Main Mall  
University of British Columbia  
Vancouver, BC, V6T 1Z1, Canada  
Telephone: 604-822-0567  
Email: [dperrin@chem.ubc.ca](mailto:dperrin@chem.ubc.ca)

Kuo-Shyan Lin, Ph.D.  
BC Cancer Research Centre  
675 West 10<sup>th</sup> Avenue  
Vancouver, BC, V5Z 1L3, Canada  
Telephone: 604-675-8203  
Email: [klin@bccrc.ca](mailto:klin@bccrc.ca)

**Running Title:**  $^{18}\text{F}$ -labeled PSMA ligands

**Word Count:** 4838 words.

## **DISCLOSURE**

This work depicts compounds pertaining to patent WO 2017/117687 A1, which entitles certain authors (H.-T. Kuo, M. Lepage, J. Pan, Z. Liu, A. Roxin, F. Bénard, K.-S. Lin, D. Perrin) to royalties upon licensing. No other potential conflicts of interest relevant to this article exist.

## ABSTRACT

Following the identification of the high-affinity glutamate-ureido scaffold, the design of several potent  $^{18}\text{F}$ - and  $^{68}\text{Ga}$ -labeled tracers has allowed spectacular progress in imaging recurrent prostate cancer by targeting the prostate specific membrane antigen (PSMA). We evaluated a series of PSMA-targeting probes that are  $^{18}\text{F}$ -labeled in a single step for PET imaging of prostate cancer. **Methods:** We prepared eight trifluoroborate constructs for prostate cancer imaging, to study the influence of the linker and the trifluoroborate prosthetic on pharmacokinetics and image quality. After one-step labeling by  $^{19}\text{F}$ - $^{18}\text{F}$  isotopic exchange, the radiotracers were injected in mice bearing LNCaP xenografts, with or without blocking controls, to assess specific uptake. PET/CT images and biodistribution data were acquired at 1 h post-injection and compared with [ $^{18}\text{F}$ ]DCFPyL on the same mouse strain and tumor model. **Results:** All tracers exhibited nanomolar affinities, were labeled in good radiochemical yields at high molar activities, and exhibited high tumor uptake in LNCaP xenografts with clearance from non-target organs. Most derivatives with a naphthylalanine linker showed significant gastrointestinal excretion. A radiotracer incorporating this linker with a dual trifluoroborate-glutamate labeling moiety showed high tumor uptake, low background activity and no liver or gastrointestinal track accumulation. **Conclusion:** PSMA-targeting probes with trifluoroborate prosthetic groups represent promising candidates for prostate cancer imaging, due to facile labeling while affording high tumor uptake values and contrast ratios that are similar to those obtained with [ $^{18}\text{F}$ ]DCFPyL.

## KEY WORDS:

PSMA,  $^{18}\text{F}$ -trifluoroborate, F-18 Labeling, Positron Emission Tomography, Prostate Cancer

## INTRODUCTION

The prostate-specific membrane antigen (PSMA), a transmembrane metalloenzyme (1), is highly overexpressed in prostate cancer and tumor-associated neovasculature (2). PSMA-targeting constructs have been designed and evaluated as imaging agents for visualizing prostate cancer, most notably by positron emission tomography (PET) (3-5). The diamino acid glutamate-ureido is commonly used for PSMA targeting due to synthetic ease, rapid pharmacokinetics, and high contrast ratios (6). [<sup>68</sup>Ga]PSMA-11 is currently the most commonly used radioligand for prostate cancer imaging (7,8). The short half-life of <sup>68</sup>Ga (68 min) generally restricts distribution to clinics that are close to a <sup>68</sup>Ge-<sup>68</sup>Ga generator, which itself limits daily production to 2 - 4 clinical doses unless direct production using a more complex solid target apparatus is implemented (9). In contrast, <sup>18</sup>F has several advantages including a longer half-life (109.8 min), higher spatial resolution than <sup>68</sup>Ga due to its short positron range, and on-demand, scalable production of [<sup>18</sup>F]fluoride ion up to a few hundred GBq (10).

To this effect, <sup>18</sup>F labeled PSMA targeting radiotracers such as [<sup>18</sup>F]DCFPyL (11) and [<sup>18</sup>F]PSMA-1007 (12) have been introduced in clinical studies. We sought to explore a new <sup>19</sup>F-<sup>18</sup>F isotope exchange (IEX) reaction on organotrifluoroborate (RBF<sub>3</sub><sup>-</sup>) groups to develop PSMA targeting radiotracers. With this approach, a precursor is converted into a radiotracer of identical chemical composition. IEX labeling of RBF<sub>3</sub><sup>-</sup> groups provides good activity yields (15-60%) and high molar activity values (≥75 GBq/μmol) (13,14). This method has been successfully applied to several [<sup>18</sup>F]RBF<sub>3</sub><sup>-</sup>-based radiotracers (14-21). We report the synthesis, radiolabeling, and PET imaging of radiotracers based on the glutamate-ureido-lysine scaffold bearing RBF<sub>3</sub><sup>-</sup> radioprosthetic groups (compounds **1–8**,

Figure 1). We measured their binding affinity toward PSMA and LogD<sub>7.4</sub> values, and then acquired PET images and *ex vivo* biodistribution data in mice bearing PSMA-expressing LNCaP prostate cancer xenografts. These results were compared with those of [<sup>18</sup>F]DCFPyL, a clinically emergent <sup>18</sup>F-labeled tracer for prostate cancer imaging.

## MATERIALS AND METHODS

### Synthesis of trifluoroborate probes and radiosynthesis

[<sup>18</sup>F]DCFPyL was prepared following literature procedures (22). Precursors for tracers **1–8** were synthesized as described in the Supplemental Data section to give azide-bearing precursors, which were conjugated to previously reported alkyne-bearing organotrifluoroborates (18). Following conjugation, the final trifluoroborate conjugate was purified by HPLC and purity was confirmed by electrospray ionisation-mass spectrometry. Representative crude and QC HPLC traces are provided in the Supplemental Data section. [<sup>18</sup>F]**1–8** were labeled *via* previously reported procedures (14,23). Briefly, 30-40 GBq of no carrier added [<sup>18</sup>F]fluoride was trapped on a QMA light cartridge and eluted with 0.9% saline or PBS (typically 100 µL) directly into a septum-sealed falcon tube containing 80–100 nmol of precursors **1–8** dissolved in 50:50 DMF-water containing 1M pyridazinium-HCl buffer (pH 2.5). The reaction was heated 80°C and a vacuum was applied to reduce the reaction volume. After 15-20 min, the reaction was quenched by addition of 2 mL of 40 mM ammonium formate or PBS and the contents were purified by semi-preparative HPLC. Radiochemical purity was confirmed by HPLC analysis using an analytical RP-C18 column with gradients of acetonitrile and water (both containing 0.1% TFA). Molar activity values were measured based on standard curve analysis.

## Cell culture

The LNCaP cell line was obtained from ATCC (LNCaP clone FGC, CRL-1740). The cells were cultured in RPMI 1640 medium supplemented with 10 % FBS, penicillin (100 U/mL) and streptomycin (100 µg/mL) at 37 °C in a MCO-19AIC (Panasonic Healthcare) humidified incubator containing 5% CO<sub>2</sub>. Cells grown to 80-90% confluence were then washed with sterile phosphate-buffered saline (1 × PBS, pH 7.4) and trypsinized. The collected cell number was counted with a Bal Supply (Sylvania, OH) 202C laboratory counter.

## *In vitro* competition binding assay

Inhibition constants ( $K_i$ ) of **1–8** and **DCFPyL** to PSMA were measured by *in vitro* competition binding assays using [<sup>18</sup>F]DCFPyL as the radioligand. LNCaP cells which were plated onto a 24-well poly-D-lysine coated plate for 48 h (400,000/well). Growth medium was removed and replaced with HEPES buffered saline (50 mM HEPES, pH 7.5, 0.9% sodium chloride) After 1 h, [<sup>18</sup>F]DCFPyL (0.1 nM) was added to each well (in triplicate) containing varied concentrations (0.5 mM – 0.05 nM) of tested compounds (**DCFPyL**, **1–8**). Non-specific binding was determined in the presence of 10 µM unlabeled **DCFPyL**. The assay mixtures were incubated for 1 h at 37 °C with gentle agitation followed by two washes with cold HEPES buffered saline. A trypsin solution (0.25 %, 400 µL) was then added to each well to harvest the cells. Radioactivity was measured by gamma counting and  $K_i$  values calculated using the 'one site - fit  $K_i$ ' built-in model in Prism 7 (GraphPad). The  $K_d$  value for [<sup>18</sup>F]DCFPyL, used for  $K_i$  determination, was 0.49 nM, as previously measured by saturation assays using LNCaP cells (24).

## Distribution Coefficient (LogD<sub>7.4</sub>) measurements

LogD<sub>7.4</sub> values were measured using the shake flask method. Briefly, an aliquot of <sup>18</sup>F-labeled tracer was added to a vial containing 2.5 mL of *n*-octanol and 2.5 mL phosphate buffer (0.1 M, pH 7.4). The mixture was vortexed for 2 min and then centrifuged at 3,000 G for 10 min. A sample of the *n*-octanol (0.1 mL) and buffer (0.1 mL) layers was counted using a gamma counter. Values of LogD<sub>7.4</sub> were calculated using the following equation:  
$$\text{LogD}_{7.4} = \log_{10} [(\text{counts in } n\text{-octanol phase})/(\text{counts in buffer phase})].$$

## PET/CT imaging and biodistribution studies

Imaging and biodistribution experiments were performed using NODSCID IL2R $\gamma$ KO male mice. All experiments were conducted according to the guidelines established by the Canadian Council on Animal Care and approved by Animal Ethics Committee of the University of British Columbia. Mice were anesthetized by inhalation with 2% isoflurane in oxygen and implanted subcutaneously with 1×10<sup>7</sup> LNCaP cells behind the left shoulder. The mice were imaged or used in biodistribution studies once the tumor reached 5-8 mm in diameter (5-6 weeks).

PET imaging experiments were conducted using an Inveon preclinical PET/CT scanner (Siemens). Compounds [<sup>18</sup>F]**1,2,3,5,7** and **8** were formulated in 10% ethanol/normal saline, while [<sup>18</sup>F]**4** and **6** were formulated in 10% ethanol/phosphate buffered saline. Each tumor bearing mouse was injected with 6 – 8 MBq of [<sup>18</sup>F]**1–8** or [<sup>18</sup>F]**DCFPyL** through the tail vein under sedation (2% isoflurane in oxygen). For blocking controls, the mice were co-injected with **DCFPyL** (0.5 mg). Following injection, the mice were allowed to recover and roam freely in their cage. After 50 min, the mice were sedated by 2% isoflurane inhalation and positioned in the scanner. A CT scan was performed first for

localization and attenuation correction. This was followed by 10-min static PET scan. The mice were kept warm by a heating pad during image acquisition. PET images were reconstructed using the IAW software (Siemens), using 2 iterations of the ordered subset expectation maximization algorithm followed by 18 iterations of the maximum *a posteriori* algorithm (OSEM/MAP).

For biodistribution and blocking studies, the mice were injected with 1-3 MBq of radiotracer. At 60 minutes, the mice were anesthetized with 2% isoflurane inhalation, and euthanized by CO<sub>2</sub> inhalation. Blood was withdrawn by cardiac puncture, and the organs/tissues of interest were collected, weighed and counted using an automatic gamma counter (PerkinElmer). Uptake values were expressed as the percentage of the injected dose per gram of tissue (%ID/g).

## **Statistical analysis**

A standard one-way ANOVA was performed to determine if statistically significant differences in tumour uptake occurred between radiotracers. Each radiotracer was compared with [<sup>18</sup>F]DCFPyL using Dunnett's test (a many-to-one *t*-test comparison). This analysis was also performed for kidney and blood activity, and tumor-to-blood and tumor-to-muscle ratios. Reported *p*-values were adjusted for multiple comparisons. The analysis was performed using Prism 8 (Graphpad).

## **RESULTS**

### **Radiolabeling**

Starting with 37 GBq of [<sup>18</sup>F]fluoride, **1–8** (80–100 nmol) were successfully labeled within 25 min with activity yields ranging from 4% to 16% (Table 1) at high molar activities ( $\geq 56$

GBq/μmol). In all cases, the radiochemical purity was ≥99% by analytical HPLC. Compounds bearing the pyridine-trifluoroborate (pyrBF<sub>3</sub>) prosthetic (**4**, **6**) were labeled in higher yields and molar activities than conjugates bearing the ammoniomethyl-trifluoroborate (AMBF<sub>3</sub>) prosthetic (**3**, **5**). Although HPLC was used to isolate tracers at ≥ 99% radiochemical purity, HPLC purification can be avoided: [<sup>18</sup>F]**6** was purified on a Sep-Pak C<sub>18</sub> cartridge according to reported procedures (23). In that case, the radiochemical purity was ≥ 95%. In addition, we deliberately labeled **2** at lower molar activity; starting with 37 GBq of NCA <sup>18</sup>F-fluoride and 1 μmol of precursor; [<sup>18</sup>F]**2** was obtained in 34% activity yield at 13.3 GBq/μmol (see **Table 2**).

## Binding assays

We determined inhibition constants *via in vitro* competition binding assays using LNCaP cells and [<sup>18</sup>F]DCFPyL as the radioligand. The K<sub>i</sub> value for DCFPyL was 2.0 ± 0.8 nM, consistent with the value previously reported by Pomper *et al.* (1.1 ± 0.1 nM) (25). Probes **1–4** and **7** had K<sub>i</sub> values in the 10–30 nM range (**Error! Reference source not found.**, top panel), while **5** and **6** had up to 10-fold better affinities, comparable to that measured for DCFPyL. Probe **8** showed excellent binding affinity to PSMA with K<sub>i</sub> value of 0.22 ± 0.01 nM (see **Table 1**).

## Distribution coefficient

All compounds but **6** had LogD<sub>7.4</sub> values similar to [<sup>18</sup>F]DCFPyL (**Error! Reference source not found.**, bottom panel). Using pyrBF<sub>3</sub> instead of AMBF<sub>3</sub> as the prosthetic group decreased hydrophilicity in **4** and **6** compared to **3** and **5**, respectively. Compound **6** was the most lipophilic compound of the series.

## PET/CT imaging and Biodistribution

Imaging [ $^{18}\text{F}$ ]DCFPyL confirmed good tumor uptake and fast clearance (25). Similarly, [ $^{18}\text{F}$ ]1–8 showed significant tumor uptake in LNCaP xenografts, that was blocked by co-injection of unlabeled DCFPyL (Figure 3), which confirmed the specificity of tumor uptake for PSMA. All images also showed high, specific kidney uptake along with urinary excretion. Bone accumulation was negligible for all radiotracers. The blocking agent caused significantly lower tumor and kidney uptake values for all compounds.

The tracers based on a naphthylalanine-tranexamic acid linker (5 and 6) displayed tumor uptake values of  $13.7 \pm 5.2$  %ID/g and  $11.9 \pm 2.3$  %ID/g respectively. [ $^{18}\text{F}$ ]1, 2, 3, 4, and 7 had uptake values of  $6.0 \pm 1.2$  %ID/g,  $8.3 \pm 1.3$  %ID/g,  $4.4 \pm 0.95$  %ID/g,  $6.3 \pm 0.8$  %ID/g, and  $5.1 \pm 1.1$  %ID/g respectively). Compounds [ $^{18}\text{F}$ ]1, 3, 4 and 7 had lower tumor uptake compared to [ $^{18}\text{F}$ ]DCFPyL (Figure 4A). Compound 8 had high tumor uptake ( $16.7 \pm 2.7$  %ID/g). No statistically significant differences were observed between compounds 2, 5 and 6 and [ $^{18}\text{F}$ ]DCFPyL, while compound 8 had higher uptake. Compounds 3 and 7 had lower kidney accumulation (Figure 4B), while compounds 5 and 6 had significantly higher intestinal activity compared to [ $^{18}\text{F}$ ]DCFPyL (Figure 4C). The blocking controls showed that intestinal uptake was not receptor mediated. The tumor-to-blood and tumor-to-muscle ratios were not statistically different from [ $^{18}\text{F}$ ]DCFPyL for any compound except compound 7, which had higher ratios (Figure 5). Compound 8, with two AMBF<sub>3</sub>-glutamate motifs, had no significant accumulation in the liver, no hepatobiliary excretion, and low background activity (Figure 6).

## DISCUSSION

We designed PSMA-targeting radiotracers that combine the advantages of one-step aqueous  $^{18}\text{F}$ -labeling afforded by two  $\text{RBF}_3^-$  radioprosthetic groups with certain chemical features found in **DCFPyL** (or its C-analogue **DCFPhL**) (4) and **PSMA-617** (26). Since the three carboxylates of Glu-ureido-Lys are needed for binding to PSMA, we introduced modifications at the lysine side chain (25,27), off of which we introduced several well-established linkers along with a suitable  $\text{RBF}_3^-$ .

Binding assays confirmed low-nanomolar affinities for compounds **5** and **6**, while compound **8** had sub-nanomolar binding affinity (**Error! Reference source not found.** and **Error! Reference source not found.A**). Compounds **1–4** exhibited 10-fold higher affinities than **DCFPyL**, suggesting that the trifluoroborate prosthetic group may not interact well with the S1 binding pocket in PSMA, which exhibits pronounced affinity for hydrophobic groups (3). Compounds incorporating a naphthylalanine-tranexamic acid motif (**5** and **6**) exhibited improved binding affinities ( $K_i = 1.14$  nM and 1.90 nM, respectively) similar to those of **DCFPyL** ( $K_i = 2.0$  nM) and **Ga-PSMA-617** ( $K_i = 2.3$  nM) (28). Interestingly, the tranexamic acid linker appears to contribute significantly to affinity as its replacement by a  $\text{PEG}_2$  spacer (compound **7**) resulted in a higher inhibition constant. The dual glutamate- $\text{BF}_3$  motif, introduced to improve the hydrophilicity of the  $\text{BF}_3$  derivatives with a naphthylalanine-tranexamic acid linker, unexpectedly improved the binding affinity of compound **8**, with a  $K_i$  approximately an order of magnitude better than **DCFPyL**.

All the  $\text{RBF}_3^-$ -bioconjugates were radiolabeled at activity yields greater than 1.85 GBq at molar activity values  $\geq 56$  GBq/ $\mu\text{mol}$  (**Error! Reference source not found.**). The  $\text{pyrBF}_3^-$ -modified conjugates showed higher activity yields compared to those modified with the

AMBF<sub>3</sub> along with higher molar activities, consistent with a report that compared both prosthetic groups in the context of LLP2A-RBF<sub>3</sub><sup>-</sup> bioconjugates (18), as well as the established stabilities of various trifluoroborates, as previously reviewed (29). High molar activities were also achieved with compound **8**, with a dual glutamate-BF<sub>3</sub> motif. Although imaging and biodistribution studies were performed with HPLC-purified tracers to ensure the highest level of purity, a simple SepPak purification of [<sup>18</sup>F]**6** (< 5 min) afforded good radiochemical purity (95%) (see Supplemental Data). This demonstrates potential for HPLC-free labeling where speed is preferred (overall synthesis time < 30 min).

While radiochemical yields were lower for certain compounds, these syntheses have not been optimized. Notably, yields were dramatically improved by increasing the amount of precursor: the lowest yield (for tracer [<sup>18</sup>F]**2**) was increased more than 8-fold to 34% when using 10 times more precursor. Consequently, the average molar activity of [<sup>18</sup>F]**2** decreased by a similar factor from 89 to 13.3 GBq/μmol. This demonstrates that yields dramatically increase when high molar activity is not critically needed.

To evaluate [<sup>18</sup>F]**1–8** for PSMA imaging, PET/CT imaging and biodistribution studies were conducted in mice bearing LNCaP tumor xenografts. Previously, Chen *et al.* and Harada *et al.* imaged [<sup>18</sup>F]**DCFPyL** in different strains of mice bearing different tumor models (25,27) thus complicating a comparison between this work and prior work. Given these discrepancies, we directly compared [<sup>18</sup>F]**1–8** with [<sup>18</sup>F]**DCFPyL** using a single mouse strain and the LNCaP xenograft tumor model as it expresses PSMA endogenously and is commonly used to evaluate PSMA-targeting radiotracers (27,28).

Imaging and biodistribution studies showed that [<sup>18</sup>F]**1–8** and [<sup>18</sup>F]**DCFPyL** were all retained in tumors and cleared from non-target tissues/organs, mainly through the renal pathway for compounds [<sup>18</sup>F]**1–4** and **8** (Error! Reference source not found.), and a

combination of renal and hepatobiliary clearance for compounds [ $^{18}\text{F}$ ]**5–7** (Figure 4). Tumor uptake was higher with [ $^{18}\text{F}$ ]**8** compared to [ $^{18}\text{F}$ ]**DCFPyL**, a result that might be explained by improved affinity. All compounds showed significant renal uptake, which was blocked by **DCFPyL**, consistent with the well-documented, high PSMA expression in mouse kidneys (25,27,28,30-33). As with [ $^{18}\text{F}$ ]**DCFPyL**, images acquired with [ $^{18}\text{F}$ ]**1–4** and **8** showed low uptake in non-target organs, while those acquired with [ $^{18}\text{F}$ ]**5–7** showed high accumulation in the gallbladder and intestines. Blocking controls showed that this intestinal uptake was not receptor mediated. While it is likely that intestinal uptake is due to the hydrophobic naphthylalanine moiety, this was not noted with  $^{68}\text{Ga}$ - or  $^{177}\text{Lu}$ -labeled PSMA-617 tracers (26). We presume that the DOTA chelator promotes renal clearance. Because many radiotracers were compared to [ $^{18}\text{F}$ ]**DCFPyL**, this study did not have statistical power to evaluate small differences between radiotracers. The results confirmed the versatility of  $\text{RBF}_3^-$  prosthetic groups for  $^{18}\text{F}$  radiolabeling, and potential strategies to direct radiotracers to favor hepatobiliary or renal clearance.

Renal clearance can be a drawback for prostate cancer imaging, as focal retention in the ureters may be confused with small nodal metastases and high bladder activity may obscure the detection of primary prostate tumors or recurrences. Conversely, excessive bowel activity may also be detrimental for detection of small lesions in the pelvis and abdomen. High liver activity, as observed in clinical studies with [ $^{18}\text{F}$ ]**DCFPyL** (11) and [ $^{18}\text{F}$ ]**PSMA-1007** (12), might impair detection of liver tumours, notably for detection of hepatocellular carcinomas where PSMA imaging may be of value (34).

Other  $^{18}\text{F}$ -labeled PSMA binding radiotracers have recently been reported, notably [ $^{18}\text{F}$ ]**PSMA-1007** (12,35), among others (36-39). The  $\text{RBF}_3^-$  radiotracers presented in this article were not directly compared with these compounds. With an excellent binding

affinity, high tumor accumulation and no liver or gastrointestinal excretion, [ $^{18}\text{F}$ ]**8** represents an attractive radiopharmaceutical for clinical translation.

## **CONCLUSION**

We report promising alternatives to current  $^{18}\text{F}$ - and  $^{68}\text{Ga}$ -labeled PSMA-targeting agents as the  $\text{RBF}_3^-$  prosthetic groups enable a facile, one-step  $^{18}\text{F}$ -labeling in aqueous media. Labeling times could be further reduced to 30 min with a simple Sep-Pak purification. The one-step labeling by IEX provided for the simple production of a precursor that is chemically identical to the radiolabeled product, simplifying aspects of both production and labeling. These radiotracers were designed to explore the influence of both the spacer and the trifluoroborate prosthetic group. Compound **8**, with a naphthylalanine-tranexamic acid linker and a dual glutamate- $\text{BF}_3$  moiety designed to enhance hydrophilicity, showed excellent binding affinity and high tumor uptake without liver accumulation or hepatobiliary clearance.

## **ACKNOWLEDGMENTS**

We thank Nadine Colpo and Navjit Hundal-Jabal for their help with the animal studies.

## REFERENCES

1. Carter RE, Feldman AR, Coyle JT. Prostate-specific membrane antigen is a hydrolase with substrate and pharmacologic characteristics of a neuropeptidase. *P Natl Acad Sci USA*. 1996;93:749-753.
2. Silver DA, Pellicer I, Fair WR, Heston WD, Cordon-Cardo C. Prostate-specific membrane antigen expression in normal and malignant human tissues. *Clin Cancer Res*. 1997;3:81-85.
3. Byun Y, Mease RC, Lupold SE, Pomper MG. Recent Development of Diagnostic and Therapeutic Agents Targeting Glutamate Carboxypeptidase II (GCPII). *Drug Design of Zinc-Enzyme Inhibitors*: John Wiley & Sons, Inc.; 2009:881-910.
4. Chen Y, Foss CA, Byun Y, et al. Radiohalogenated Prostate-Specific Membrane Antigen (PSMA)-Based Ureas as Imaging Agents for Prostate Cancer. *J Med Chem*. 2008;51:7933-7943.
5. Maurer T, Eiber M, Schwaiger M, Gschwend JE. Current use of PSMA - PET in prostate cancer management. *Nat Rev Urol*. 2016;13:226-235.
6. Kiess AP, Banerjee SR, Mease RC, et al. Prostate-specific membrane antigen as a target for cancer imaging and therapy. *Q J Nucl Med Mol Imaging*. 2015;59:241-268.
7. Lutje S, Heskamp S, Cornelissen AS, et al. PSMA Ligands for Radionuclide Imaging and Therapy of Prostate Cancer: Clinical Status. *Theranostics*. 2015;5:1388-1401.
8. Calais J, Fendler WP, Herrmann K, Eiber M, Ceci F. Comparison of <sup>68</sup>Ga-PSMA-11 and <sup>18</sup>F-Fluciclovine PET/CT in a Case Series of 10 Patients with Prostate Cancer Recurrence. *J Nucl Med*. 2018;59:789-794.
9. Lin M, Waligorski GJ, Lepera CG. Production of curie quantities of Ga-68 with a medical cyclotron via the Zn-68 (p,n)Ga-68 reaction. *Appl Radiat Isotopes*. 2018;133:1-3.
10. Eberl S, Eriksson T, Svedberg O, et al. High beam current operation of a PETtrace (TM) cyclotron for F-18(-) production. *Appl Radiat Isotopes*. 2012;70:922-930.
11. Szabo Z, Mena E, Rowe SP, et al. Initial Evaluation of [(18)F]DCFPyL for Prostate-Specific Membrane Antigen (PSMA)-Targeted PET Imaging of Prostate Cancer. *Mol Imaging Biol*. 2015;17:565-574.
12. Giesel FL, Hadaschik B, Cardinale J, et al. F-18 labelled PSMA-1007: biodistribution, radiation dosimetry and histopathological validation of tumor lesions in prostate cancer patients. *Eur J Nucl Med Mol Imaging*. 2017;44:678-688.

13. Liu Z, Li Y, Lozada J, Lin K-S, Schaffer P, Perrin DM. Rapid, One-Step, High Yielding  $^{18}\text{F}$ -Labeling of an Aryltrifluoroborate Bioconjugate by Isotope Exchange at Very High Specific Activity, . *J Labelled Comp Radiopharm*. 2012;14:491-497.
14. Liu ZB, Pourghiasian M, Radtke MA, et al. An Organotrifluoroborate for Broadly Applicable One-Step F-18-Labeling. *Angew Chem Int Ed Engl*. 2014;53:11876-11880.
15. Zhang ZX, Jenni S, Zhang CC, et al. Synthesis and evaluation of F-18-trifluoroborate derivatives of triphenylphosphonium for myocardial perfusion imaging. *Bioorg Med Chem Lett*. 2016;26:1675-1679.
16. Lau J, Liu ZB, Lin KS, et al. Trimeric Radiofluorinated Sulfonamide Derivatives to Achieve In Vivo Selectivity for Carbonic Anhydrase IX-Targeted PET Imaging. *J Nucl Med*. 2015;56:1434-1440.
17. Liu Z, Radtke MA, Wong MQ, Lin K-S, Yapp DT, Perrin DM. Dual Mode Fluorescent ( $^{18}\text{F}$ )-PET Tracers: Efficient Modular Synthesis of Rhodamine- cRGD 2- ( $^{18}\text{F}$ ) - Organotrifluoroborate, Rapid, and High Yielding One-Step ( $^{18}\text{F}$ )-Labeling at High Specific Activity, and Correlated in Vivo PET Imaging and ex Vivo Fluorescence. *Bioconjug Chem*. 2014;25:1951-1962.
18. Roxin Á, Zhang C, Huh S, et al. Preliminary evaluation of  $^{18}\text{F}$ -labeled LLP2A-trifluoroborate conjugates as VLA-4 ( $\alpha_4\beta_1$  integrin) specific radiotracers for PET imaging of melanoma. *Nucl Med Biol*. 2018;61:11-20.
19. Zhang C, Zhang Z, Lin K-S, et al. Melanoma Imaging Using  $^{18}\text{F}$ -Labeled alpha-Melanocyte-Stimulating Hormone Derivatives with Positron Emission Tomography. *Mol Pharm*. 2018;15:2116-2122.
20. Pourghiasian M, Liu ZB, Pan JH, et al. F-18-AmBF3-MJ9: A novel radiofluorinated bombesin derivative for prostate cancer imaging. *Bioorg Med Chem*. 2015;23:1500-1506.
21. Liu ZB, Amouroux G, Zhang ZX, et al. F-18-Trifluoroborate Derivatives of Des-Arg(10) Kallidin for Imaging Bradykinin B1 Receptor Expression with Positron Emission Tomography. *Mol Pharm*. 2015;12:974-982.
22. Bouvet V, Wuest M, Jans H-S, et al. Automated synthesis of [ $^{18}\text{F}$ ]DCFPyL via direct radiofluorination and validation in preclinical prostate cancer models. *Ejnmri Res*. 2016;6:40.
23. Liu ZB, Lin KS, Benard F, et al. One-step F-18 labeling of biomolecules using organotrifluoroborates. *Nat Protoc*. 2015;10:1423-1432.
24. Kuo HT, Pan J, Zhang Z, et al. Effects of linker modification on tumor-to-kidney contrast of  $^{68}\text{Ga}$ -labeled PSMA-targeted imaging probes. *Mol Pharm*. 2018; 15:3502-3511.

- 25.** Chen Y, Pullambhatla M, Foss CA, et al. 2-(3-{1-Carboxy-5-[(6-[18F]Fluoro-Pyridine-3-Carbonyl)-Amino]-Pentyl}-Ureido)-Pentanedioic Acid, [18F]DCFPyL, a PSMA-Based PET Imaging Agent for Prostate Cancer. *Clin Cancer Res.* 2011;17:7645-7653.
- 26.** Kratochwil C, Giesel FL, Eder M, et al. [(1)(7)(7)Lu]Lutetium-labelled PSMA ligand-induced remission in a patient with metastatic prostate cancer. *Eur J Nucl Med Mol Imaging.* 2015;42:987-988.
- 27.** Harada N, Kimura H, Onoe S, et al. Synthesis and Biologic Evaluation of Novel F-18-Labeled Probes Targeting Prostate-Specific Membrane Antigen for PET of Prostate Cancer. *J Nucl Med.* 2016;57:1978-1984.
- 28.** Benesova M, Schafer M, Bauder-Wust U, et al. Preclinical Evaluation of a Tailor-Made DOTA-Conjugated PSMA Inhibitor with Optimized Linker Moiety for Imaging and Endoradiotherapy of Prostate Cancer. *J Nucl Med.* 2015;56:914-920.
- 29.** Perrin DM. F-18 -Organotrifluoroborates as Radioprosthetic Groups for PET Imaging: From Design Principles to Preclinical Applications. *Accounts Chem Res.* 2016;49:1333-1343.
- 30.** Weineisen M, Schottelius M, Simecek J, et al. Ga-68- and Lu-177-Labeled PSMA I&T: Optimization of a PSMA-Targeted Theranostic Concept and First Proof-of-Concept Human Studies. *J Nucl Med.* 2015;56:1169-1176.
- 31.** Gregor PD, Wolchok JD, Turaga V, et al. Induction of autoantibodies to syngeneic prostate-specific membrane antigen by xenogeneic vaccination. *Int J Cancer.* 2005;116:415-421.
- 32.** Schmittgen TD, Zakrajsek BA, Hill RE, et al. Expression pattern of mouse homolog of prostate-specific membrane antigen (FOLH1) in the transgenic adenocarcinoma of the mouse prostate model. *Prostate.* 2003;55:308-316.
- 33.** Yang DM, Holt GE, Velders MP, Kwon ED, Kast WM. Murine six-transmembrane epithelial antigen of the prostate, prostate stem cell antigen, and prostate-specific membrane antigen: Prostate-specific cell-surface antigens highly expressed in prostate cancer of transgenic adenocarcinoma mouse prostate mice. *Cancer Res.* 2001;61:5857-5860.
- 34.** Kesler M, Levine C, Hershkovitz D, et al. (68)Ga-PSMA is a novel PET-CT tracer for imaging of hepatocellular carcinoma: A prospective pilot study. *J Nucl Med.* 2018. doi: 10.2967/jnumed.118.214833. [Epub ahead of print].
- 35.** Cardinale J, Schafer M, Benesova M, et al. Preclinical Evaluation of (18)F-PSMA-1007, a New Prostate-Specific Membrane Antigen Ligand for Prostate Cancer Imaging. *J Nucl Med.* 2017;58:425-431.

- 36.** Rowe SP, Gage KL, Faraj SF, et al. (1)(8)F-DCFBC PET/CT for PSMA-Based Detection and Characterization of Primary Prostate Cancer. *J Nucl Med.* 2015;56:1003-1010.
- 37.** Malik N, Baur B, Winter G, Reske SN, Beer AJ, Solbach C. Radiofluorination of PSMA-HBED via Al(18)F(2+) Chelation and Biological Evaluations In Vitro. *Mol Imaging Biol.* 2015;17:777-785.
- 38.** Behr SC, Aggarwal R, Van Brocklin HF, et al. First-in-Human Phase I study of CTT1057, a Novel (18)F Labeled Imaging Agent with Phosphoramidate Core Targeting Prostate Specific Membrane Antigen in Prostate Cancer. *J Nucl Med.* 2018; doi: 10.2967/jnumed.118.220715. [Epub ahead of print].
- 39.** Zlatopolskiy BD, Endepols H, Krapf P, et al. Discovery of (18)F-JK-PSMA-7, a novel PET-probe for the detection of small PSMA positive lesions. *J Nucl Med.* 2018; doi: 10.2967/jnumed.118.218495. [Epub ahead of print]

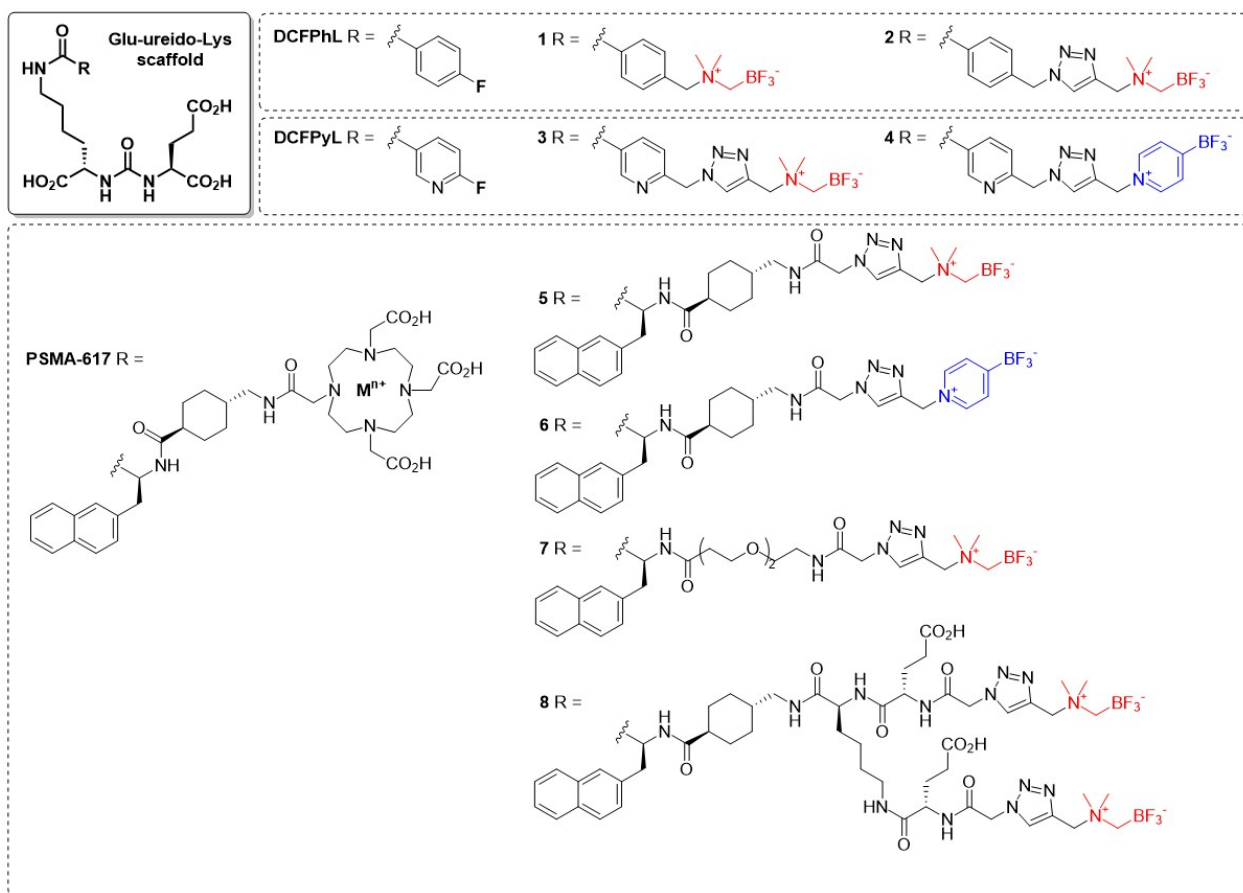


**Figure 1.** Trifluoroborate probes resembling the scaffolds of **DCFPyL**, **DCFPyL** and **PSMA-617**. In **red**:  $\text{AMBF}_3$  prosthetic; in **blue**:  $\text{pyrBF}_3$  prosthetic.

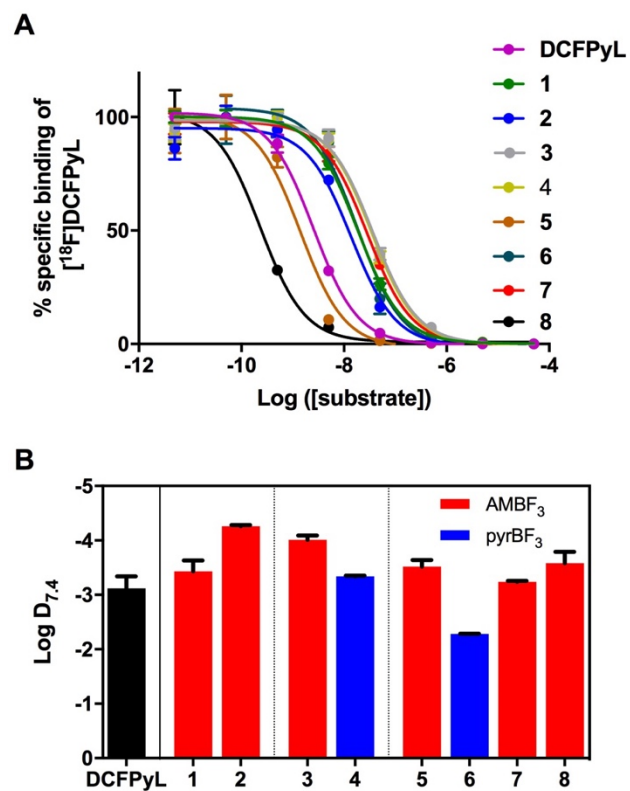


**Figure 2.** (A) Competitive inhibition curves of **DCFPyL** and **1–8**. (B) Values of distribution coefficient (Log D<sub>7.4</sub>) for **DCFPyL** and **1–8** (error bars reflect standard deviations).

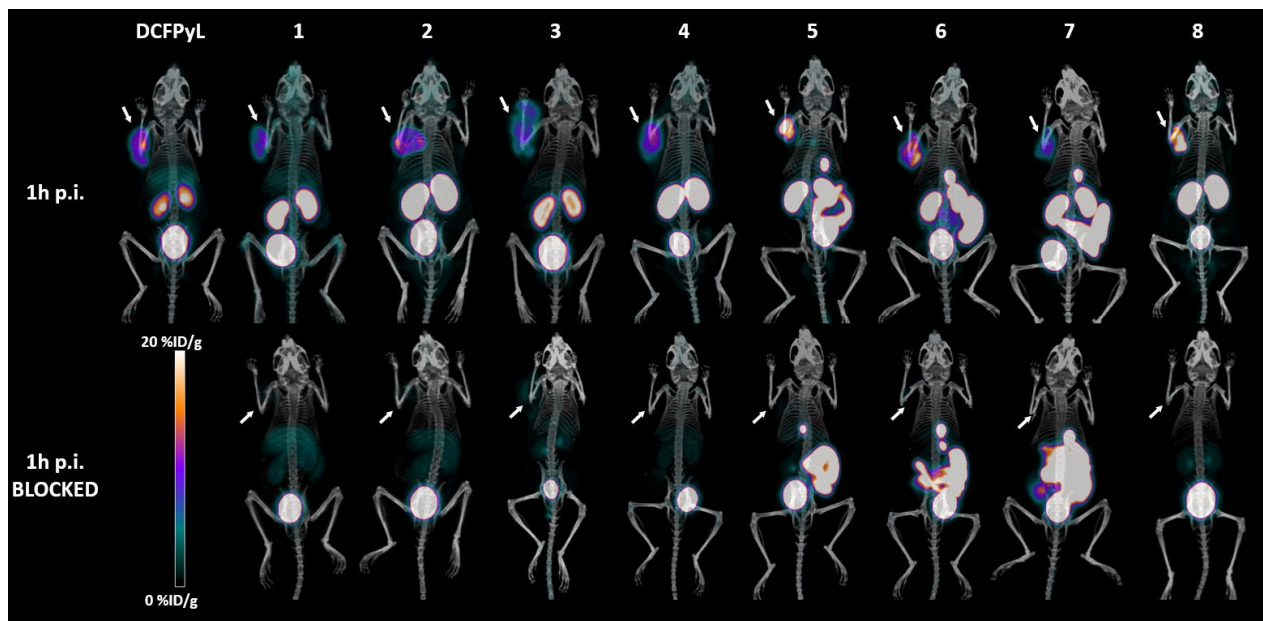


**Figure 3.** PET/CT images (maximum intensity projections) of LNCaP tumor bearing mice at 1 h p.i., with and without blocking by co-injection of unlabeled **DCFPyL**. The white arrows locate tumors.

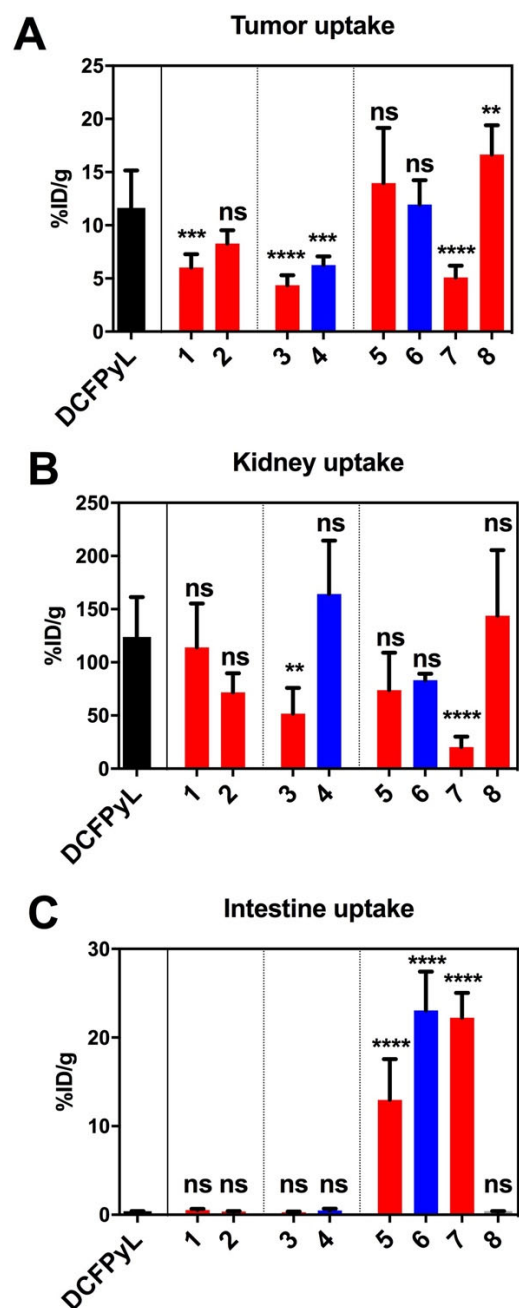


**Figure 4.** Uptake values for tumor (panel A), kidney (B), and intestine (C) for compounds 1–8 and DCFPyL; in black: DCFPyL; in red: AMBF<sub>3</sub> derivatives; in blue: pyrBF<sub>3</sub> derivatives (error bars reflect standard deviation values, significance of differences with [<sup>18</sup>F]DCFPyL indicated at top of bars: \*\**p* < 0.01; \*\*\*\**p* < 0.0001; ns = not significant). Full data available in the Supplemental Data section.

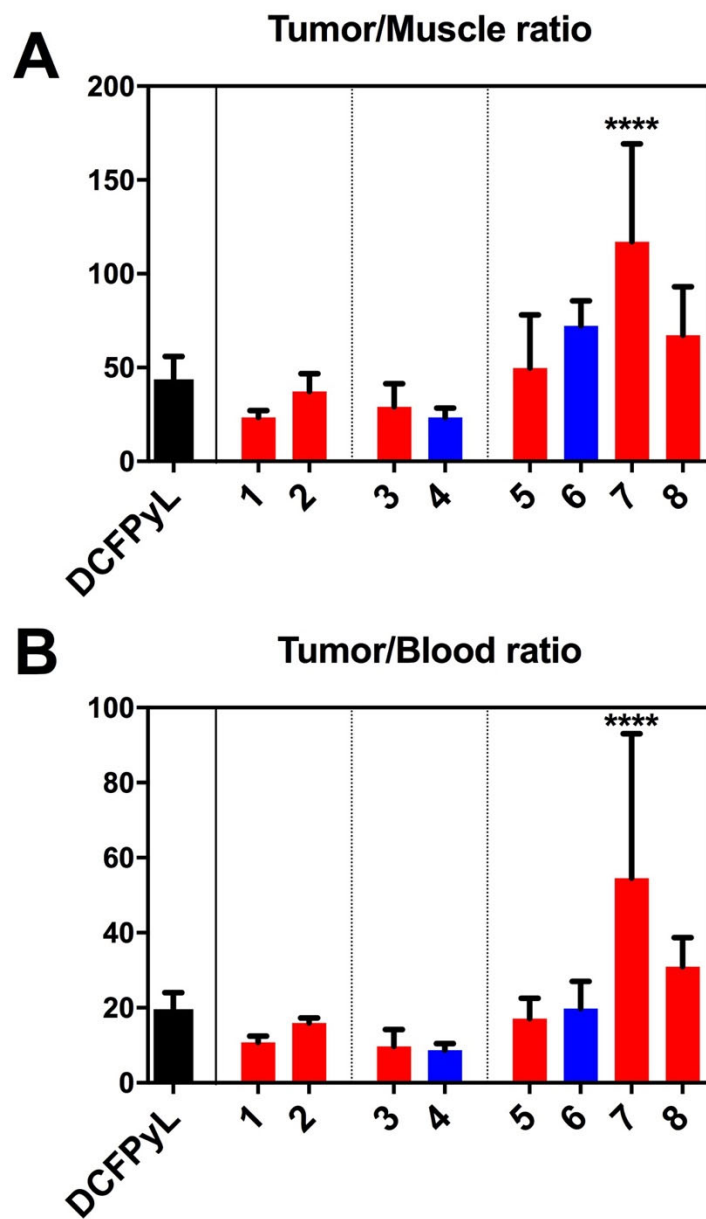


**Figure 5.** Contrast ratios (tumor-to-muscle in panel A and tumor-to-blood, panel B) for compounds 1–8 and DCFPyL at 1 h p.i.; in **black**: DCFPyL; in **red**: AMBF<sub>3</sub> derivatives; in **blue**: pyrBF<sub>3</sub> derivatives (error bars reflect standard deviation values, significance of differences with [<sup>18</sup>F]DCFPyL indicated at top of bars: \*\*\*\* $p < 0.0001$ ).

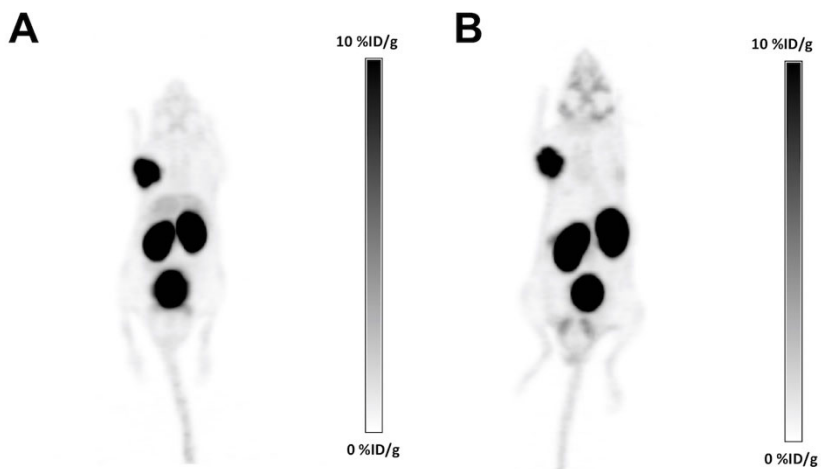


**Figure 6.** PET/CT images (maximum intensity projections in black on white to display background activity), comparing [<sup>18</sup>F]DCFPyL (A) with [<sup>18</sup>F]8 (B), showing similar image contrast with lower liver accumulation for compound **8**. The maximum of the scale corresponds to 10 %ID/g for both radiotracers.

**Table 1.**

<b>Tracer</b>	<b>Activity Yield* (%, isolated)</b>	<b>Molar activity† (GBq/μmol)</b>	<b>LogD<sub>7.4</sub> (n = 3)</b>	<b>K<sub>i</sub> (nM) (n = 3)</b>
<b>[<sup>18</sup>F]DCFPyL</b>	12 ± 3 (n = 7)	118 ± 37 (n = 7)	-3.12 ± 0.22	2.0 ± 0.8
<b>[<sup>18</sup>F]1</b>	7 ± 4 (n = 4)	70 ± 19 (n = 4)	-3.43 ± 0.35	14.4 ± 2.7
<b>[<sup>18</sup>F]2</b>	4 ± 2 (n = 3)	89 ± 26 (n = 3)	-4.26 ± 0.04	11.8 ± 0.9
<b>[<sup>18</sup>F]3</b>	5 ± 1 (n = 3)	56 ± 15 (n = 3)	-4.01 ± 0.14	25.9 ± 5.7
<b>[<sup>18</sup>F]4</b>	16 ± 2 (n = 3)	148 ± 89 (n = 3)	-3.34 ± 0.02	27.6 ± 3.8
<b>[<sup>18</sup>F]5</b>	13 ± 10 (n = 2)	137 ± 22 (n = 2)	-3.52 ± 0.21	1.14 ± 0.26
<b>[<sup>18</sup>F]6</b>	15 ± 2 (n = 6)	278 ± 73 (n = 6)	-2.28 ± 0.01	1.90 ± 0.68
<b>[<sup>18</sup>F]7</b>	10 ± 5 (n = 3)	92 ± 22 (n = 2)	-3.24 ± 0.03	16.5 ± 5.5
<b>[<sup>18</sup>F]8</b>	7 ± 6 (n = 3)	211 ± 48 (n = 3)	-3.58 ± 0.36	0.22 ± 0.01

\*Activity yields are reported at end of synthesis (1 h for **DCFPyL**, 40 min for **1-8**) (with no correction for decay).

†Molar activities are reported at time of QC injection, shortly following end of synthesis.

**Table 2.**

<b>Tracers</b>	<b>Activity Yield (%)</b>	<b>Molar activity (GBq/μmol)</b>
[ <sup>18</sup> F]2 from 100 nmol (n = 3)	4 ± 2	89 ± 26
[ <sup>18</sup> F]2 from 1000 nmol (n = 2)	34 ± 9	13.3 ± 0.74
Change	x 8.5	÷ 6.7

## One-step $^{18}\text{F}$ -labeling and preclinical evaluation of PSMA-targeting trifluoroborate probes: varying structure and prosthetic group for prostate cancer imaging

Hsiou-Ting Kuo<sup>1,2,‡</sup>, Mathieu L. Lepage<sup>3</sup>, Kuo-Shyan Lin<sup>1,2,\*</sup>, Jinhe Pan<sup>1</sup>, Zhengxing Zhang<sup>1</sup>, Zhibo Liu<sup>3</sup>, Alla Pryyma<sup>3</sup>, Chengcheng Zhang<sup>1</sup>, Helen Merkens<sup>1,2</sup>, Aron Roxin<sup>1,3</sup>, David M. Perrin<sup>3,\*</sup>, François Bénard<sup>1,2,\*</sup>

<sup>a</sup> University of British Columbia, Chemistry Department, 2036 Main Mall, Vancouver, BC V6T1Z1, Canada.

<sup>b</sup> BC Cancer Research Center, 675 W 10th Ave, Vancouver, BC V5Z1L3, Canada.

<sup>‡</sup> M.L. Lepage and H.-T. Kuo contributed equally to this manuscript.

\* Corresponding authors.

### Supplemental Data

#### COMPARATIVE QC ANALYSIS OF TRACER [ $^{18}\text{F}$ ]6 PURIFIED BY SEMI-PREPARATIVE HPLC OR SEP-PAK C<sub>18</sub> TRAPPING

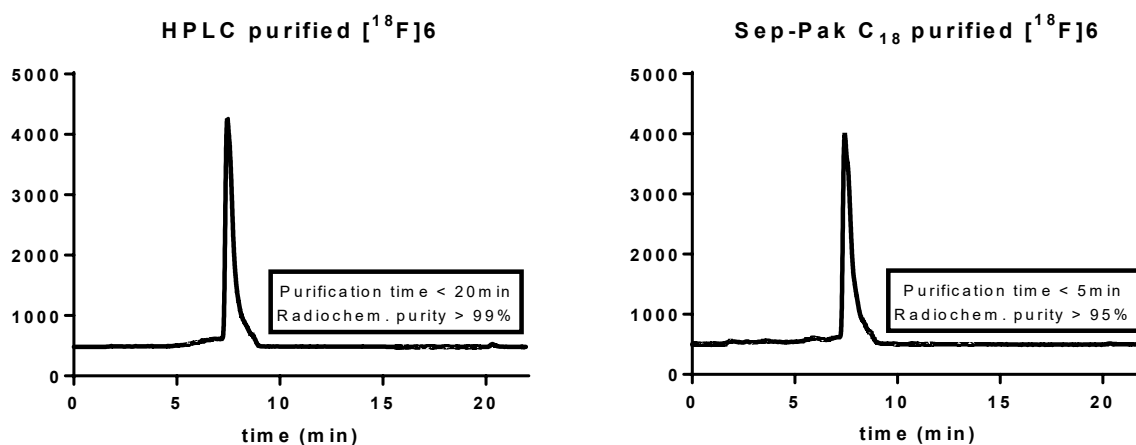


**Figure S 1** – Comparative QC analysis of tracer [ $^{18}\text{F}$ ]6 purified by semi-preparative HPLC (left) or Sep-Pak C<sub>18</sub> trapping.

**COMPLETE BIODISTRIBUTION STUDIES****Statistical analysis**

Statistical analyses were performed using GradPad prism 7. Multiple *t* tests were performed to compare biodistribution in unblocked and blocked mice, multiple comparisons were corrected using the Holm-Sidak method. The difference was considered statistically significant when *p* value was < 0.05.

**Table S 1** – Complete biodistribution study for compounds [<sup>18</sup>F]1–3

Tissue (%ID/g)	[ <sup>18</sup> F]1		[ <sup>18</sup> F]2		[ <sup>18</sup> F]3	
	1h n = 8	1h blocked n = 4	1h n = 6	1h blocked n = 4	1h n = 8	1h blocked n = 5
<b>blood</b>	0.57 ± 0.15	0.45 ± 0.27	0.52 ± 0.06	0.46 ± 0.24	0.50 ± 0.16	0.30 ± 0.10
<b>fat</b>	0.99 ± 0.39	0.14 ± 0.08*	0.73 ± 0.26	0.06 ± 0.01**	0.35 ± 0.15	0.16 ± 0.10
<b>testes</b>	0.62 ± 0.15	0.10 ± 0.02***	0.67 ± 0.17	0.08 ± 0.02**	0.30 ± 0.09	0.10 ± 0.03**
<b>intestine</b>	0.54 ± 0.11	0.57 ± 0.23	0.33 ± 0.05	0.31 ± 0.02	0.28 ± 0.07	0.23 ± 0.06
<b>stomach</b>	0.12 ± 0.05	0.11 ± 0.08	0.10 ± 0.03	0.06 ± 0.02	0.08 ± 0.04	0.06 ± 0.02
<b>spleen</b>	2.67 ± 0.98	0.13 ± 0.03**	5.01 ± 0.64	0.09 ± 0.03***	0.84 ± 0.52	0.09 ± 0.05
<b>liver</b>	2.90 ± 0.56	3.00 ± 0.53	1.69 ± 0.19	1.76 ± 0.17	1.17 ± 0.28	1.25 ± 0.17
<b>pancreas</b>	0.55 ± 0.16	0.11 ± 0.03**	0.33 ± 0.05	0.06 ± 0.01***	0.27 ± 0.13	0.08 ± 0.03
<b>adrenal</b>	4.77 ± 1.75	0.35 ± 0.14**	4.65 ± 1.75	0.20 ± 0.05**	1.35 ± 0.52	0.24 ± 0.07**
<b>kidney</b>	114.00 ± 41.30	3.54 ± 0.83**	71.70 ± 18.0	2.11 ± 0.19***	51.80 ± 24.10	2.12 ± 0.73*
<b>lung</b>	1.37 ± 0.36	0.25 ± 0.06**	1.39 ± 0.17	0.22 ± 0.03***	0.66 ± 0.19	0.30 ± 0.11*
<b>heart</b>	0.30 ± 0.06	0.15 ± 0.04*	0.33 ± 0.08	0.09 ± 0.02**	0.19 ± 0.07	0.12 ± 0.06
<b>tumor</b>	<b>6.04 ± 1.24</b>	<b>0.33 ± 0.07***</b>	<b>8.28 ± 1.25</b>	<b>0.27 ± 0.06***</b>	<b>4.36 ± 0.95</b>	<b>0.35 ± 0.21***</b>
<b>muscle</b>	0.26 ± 0.08	0.13 ± 0.03	0.23 ± 0.04	0.12 ± 0.05*	0.17 ± 0.07	0.09 ± 0.03
<b>bone</b>	0.36 ± 0.02	0.30 ± 0.07	0.44 ± 0.09	0.30 ± 0.06	0.20 ± 0.06	0.16 ± 0.06
<b>brain</b>	0.04 ± 0.01	0.03 ± 0.01	0.04 ± 0.01	0.02 ± 0.00*	0.03 ± 0.01	0.02 ± 0.00
<b>T/M</b>	23.43 ± 3.71	2.63 ± 1.10***	37.30 ± 9.53	2.66 ± 1.60**	29.00 ± 12.40	3.54 ± 1.43*
<b>T/B</b>	10.82 ± 1.64	0.91 ± 0.44***	15.95 ± 1.37	0.77 ± 0.48***	9.68 ± 4.53	1.17 ± 0.70*
<b>T/K</b>	0.07 ± 0.06	0.10 ± 0.03	0.12 ± 0.04	0.13 ± 0.02	0.11 ± 0.08	0.16 ± 0.05

Significance of differences between unblocked and blocked groups: \**p* < 0.05; \*\**p* < 0.01; \*\*\**p* < 0.001.

**Table S 2** – Complete biodistribution study for compounds [<sup>18</sup>F]4–6.

Tissue (%ID/g)	[ <sup>18</sup> F]4		[ <sup>18</sup> F]5		[ <sup>18</sup> F]6	
	1h n = 7	1h blocked n = 4	1h n = 6	1h blocked n = 4	1h n = 5	1h blocked n = 4
<b>blood</b>	0.74 ± 0.15	0.24 ± 0.11**	0.89 ± 0.42	0.44 ± 0.02	0.68 ± 0.26	1.64 ± 2.58
<b>fat</b>	1.05 ± 0.49	0.04 ± 0.03*	0.83 ± 0.33	0.16 ± 0.06	0.38 ± 0.14	0.06 ± 0.02*
<b>testes</b>	0.67 ± 0.27	0.08 ± 0.03*	0.74 ± 0.55	0.24 ± 0.05	0.33 ± 0.05	0.14 ± 0.04**
<b>intestine</b>	0.48 ± 0.22	0.18 ± 0.04	12.96 ± 4.61	12.36 ± 0.55	23.05 ± 4.39	24.50 ± 4.86
<b>stomach</b>	0.15 ± 0.03	0.06 ± 0.02**	0.37 ± 0.45	0.12 ± 0.10	1.17 ± 1.35	0.88 ± 0.41
<b>spleen</b>	3.36 ± 1.08	0.13 ± 0.06**	3.21 ± 1.73	0.21 ± 0.02	1.77 ± 0.70	0.18 ± 0.10*
<b>liver</b>	1.28 ± 0.18	0.90 ± 0.25	1.14 ± 0.48	0.67 ± 0.13	0.98 ± 0.22	0.87 ± 0.17
<b>pancreas</b>	0.68 ± 0.50	0.08 ± 0.03	0.30 ± 0.17	0.13 ± 0.06	0.26 ± 0.06	0.16 ± 0.14
<b>adrenal</b>	6.66 ± 2.33	0.26 ± 0.15**	2.89 ± 1.94	0.34 ± 0.09	2.14 ± 0.61	0.20 ± 0.04**
<b>kidney</b>	164.33 ± 50.20	1.62 ± 0.73**	73.86 ± 35.21	1.04 ± 0.14	83.22 ± 6.07	1.30 ± 0.25***
<b>lung</b>	1.67 ± 0.47	0.19 ± 0.09**	1.21 ± 0.48	0.39 ± 0.01	1.05 ± 0.14	0.43 ± 0.23*
<b>heart</b>	0.34 ± 0.08	0.09 ± 0.04**	0.31 ± 0.11	0.15 ± 0.00	0.22 ± 0.03	0.17 ± 0.07
<b>tumor</b>	<b>6.26 ± 0.82</b>	<b>0.18 ± 0.11***</b>	<b>13.96 ± 5.20</b>	<b>0.41 ± 0.04*</b>	<b>11.94 ± 2.29</b>	<b>0.37 ± 0.10***</b>
<b>muscle</b>	0.28 ± 0.07	0.11 ± 0.08*	0.36 ± 0.18	0.15 ± 0.02	0.17 ± 0.02	0.10 ± 0.02*
<b>bone</b>	0.76 ± 0.57	0.56 ± 0.20	0.34 ± 0.14	0.17 ± 0.03	0.56 ± 0.14	0.57 ± 0.37
<b>brain</b>	0.05 ± 0.01	0.02 ± 0.01**	0.04 ± 0.01	0.02 ± 0.00	0.03 ± 0.01	0.03 ± 0.03
<b>T/M</b>	23.40 ± 5.00	1.91 ± 0.46***	49.67 ± 28.45	2.85 ± 0.70	72.20 ± 13.46	3.78 ± 0.17**
<b>T/B</b>	8.70 ± 1.74	0.75 ± 0.18***	17.12 ± 5.40	0.95 ± 0.10**	19.80 ± 7.23	0.72 ± 0.43*
<b>T/K</b>	0.04 ± 0.02	0.11 ± 0.03**	0.21 ± 0.08	0.41 ± 0.09	0.14 ± 0.02	0.29 ± 0.07*

Significance of differences between unblocked and blocked groups: \* $p < 0.05$ ; \*\* $p < 0.01$ ; \*\*\* $p < 0.001$ .

**Table S 3** – Complete biodistribution study for compounds [<sup>18</sup>F]7–8 and [<sup>18</sup>F]DCFPyL

Tissue (%ID/g)	<sup>18</sup> F]7		<sup>18</sup> F]8		<sup>18</sup> F]DCFPyL
	1h n = 6	1h blocked n = 4	1h n = 8	1h blocked n = 4	1h n = 8
blood	0.13 ± 0.08	0.85 ± 1.37	0.56 ± 0.11	0.39 ± 0.07*	0.60 ± 0.13
fat	0.27 ± 0.14	0.02 ± 0.02	0.80 ± 0.28	0.06 ± 0.02***	1.05 ± 0.64
testes	0.18 ± 0.05	0.04 ± 0.01**	0.57 ± 0.12	0.18 ± 0.09***	0.57 ± 0.21
intestine	22.24 ± 2.79	26.68 ± 9.98	0.32 ± 0.06	0.26 ± 0.05	0.33 ± 0.07
stomach	0.21 ± 0.12	1.55 ± 2.10	0.11 ± 0.03	0.09 ± 0.04	0.12 ± 0.03
spleen	0.75 ± 0.36	0.15 ± 0.16	6.47 ± 2.17	0.12 ± 0.04***	3.98 ± 2.35
liver	0.83 ± 0.34	0.73 ± 0.21	0.20 ± 0.05	0.16 ± 0.04	1.82 ± 0.24
pancreas	0.13 ± 0.11	0.06 ± 0.06	0.46 ± 0.15	0.09 ± 0.03***	0.58 ± 0.32
adrenal	0.81 ± 0.25	0.06 ± 0.09**	7.72 ± 2.70	0.14 ± 0.03***	3.02 ± 2.14
kidney	20.35 ± 9.85	0.56 ± 0.18	143.85 ± 61.73	2.19 ± 0.44**	123.76 ± 37.67
lung	0.40 ± 0.13	0.12 ± 0.04*	1.97 ± 0.34	0.33 ± 0.06***	1.62 ± 0.68
heart	0.07 ± 0.02	0.04 ± 0.01	0.28 ± 0.07	0.13 ± 0.01**	0.35 ± 0.12
tumor	<b>5.09 ± 1.10</b>	<b>0.15 ± 0.06***</b>	<b>16.66 ± 2.74</b>	<b>0.35 ± 0.03***</b>	<b>11.64 ± 3.52</b>
muscle	0.05 ± 0.01	0.24 ± 0.37	0.27 ± 0.06	0.13 ± 0.06**	0.29 ± 0.12
bone	0.10 ± 0.07	0.16 ± 0.25	0.25 ± 0.10	0.15 ± 0.02	0.33 ± 0.07
brain	0.01 ± 0.01	0.01 ± 0.01	0.02 ± 0.00	0.01 ± 0.00***	0.03 ± 0.01
T/M	117.13 ± 52.06	3.62 ± 3.62*	67.23 ± 25.93	3.07 ± 0.92***	43.67 ± 12.21
T/B	54.57 ± 38.49	1.56 ± 0.87	30.95 ± 7.76	0.92 ± 0.24***	19.64 ± 4.41
T/K	0.28 ± 0.22	0.28 ± 0.12	0.14 ± 0.07	0.17 ± 0.04	0.10 ± 0.02

Significance of differences between unblocked and blocked groups: \**p* < 0.05; \*\**p* < 0.01; \*\*\**p* < 0.001.

### IN VITRO PLASMA STABILITY STUDY

*In vitro* stability of [<sup>18</sup>F]1–8 and [<sup>18</sup>F]DCFPyL was conducted in balb/c mouse plasma following previously published procedures (1,2), and monitored by radio-HPLC using the semi-preparative column eluted with various gradients of water/acetonitrile (0.1% TFA). No change in retention time was observed over the course of the study. Neither degradation nor release of free <sup>18</sup>F-fluoride was detected.

### SYNTHESIS OF COLD PRECURSORS

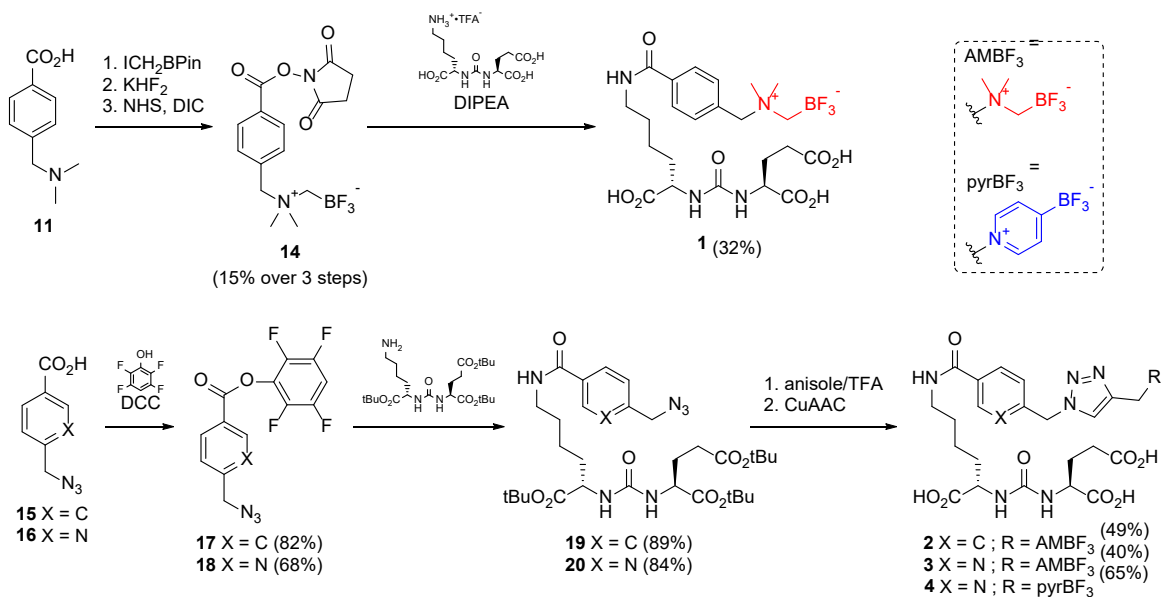
#### Chemicals and instrumentation

Glu-ureido-Lys trifluoroacetate, *t*-butyl protected Glu-ureido-Lys (OtBu-Glu(OtBu)-ureido-Lys-OtBu), methyl 4-[(dimethylamino)methyl]benzoate (**11**), 4-azidomethylbenzoic acid (**15**), 4-azidomethylnicotinic acid (**16**), *N*-propargyl-*N,N*-dimethylammoniummethyltrifluoroborate, *N*-propargylpyridinium *para*-trifluoroborate, DCFPyL and its fluorination precursor (S)-2-[3-[(S)-1-carboxy-5-(6-trimethylammonium-pyridine-3-carboxamido)pentyl]ureido]pentanedioic acid trifluoroacetate salt were prepared according to literature procedures (1-7). All other chemicals and solvents were obtained from commercial sources, and used without further purification. Purification and quality control of cold and radiolabeled PSMA-targeting peptidomimetics were

performed on Agilent HPLC systems equipped with a model 1200 quaternary pump, a model 1200 UV absorbance detector (set at 220 nm), and a Bioscan (Washington, DC) NaI scintillation detector. The operation of Agilent HPLC systems was controlled using the Agilent ChemStation software. The HPLC columns used were a Phenomenex (Torrance, CA) Luna C<sub>18</sub> semi-preparative column (5 μ, 250 × 10 mm), a Phenomenex Luna C<sub>18</sub> analytical column (5 μ, 250 × 4.6 mm), or a Phenomenex Jupiter C<sub>18</sub> analytical column (10 μ, 250 × 4.6 mm). Lyophilization was conducted using a Labconco (Kansas City, MO) FreeZone 4.5 Plus freeze-drier. Mass analyses were performed using a Bruker (Billerica, MA) Esquire-LC/MS system with ESI ion source. Anion exchange columns were purchased from ORTG Inc. (Orkdale, TN), and C<sub>18</sub> Sep-Pak cartridges (1 cm<sup>3</sup>, 50 mg) were obtained from Waters (Milford, MA). <sup>18</sup>F-Fluoride was produced by the <sup>18</sup>O(p, n)<sup>18</sup>F reaction using an Advanced Cyclotron Systems Inc. (Richmond, Canada) TR19 cyclotron. Radioactivity of <sup>18</sup>F-labeled tracers was measured using a Capintec (Ramsey, NJ) CRC<sup>®</sup>-25R/W dose calibrator, and the radioactivity of mouse tissues collected from biodistribution studies were counted using a Perkin Elmer (Waltham, MA) Wizard2 2480 automatic gamma counter.

### Synthesis of precursors (Figure S 2)

Compound **1** was prepared by coupling of the Glu-Lys ureido scaffold with a modified benzoic derivative: 4-[(dimethylamino)methyl]benzoate **11** was directly alkylated with (iodomethyl)boronic pinacol ester, which was then converted to the zwitterionic trifluoroborate. The coupling between the corresponding NHS ester **14** with deprotected Glu-ureido-Lys backbone (TFA salt) afforded **1**. Compounds **2-4** were prepared from azide-armed Glu-ureido-Lys scaffolds **19** and **20** (themselves prepared in similar fashion than **1**), onto which was attached the desired trifluoroborate (AMBF<sub>3</sub> or pyrBF<sub>3</sub>) prosthetic *via* CuAAC. In a similar approach, the coupling of the desired prosthetic onto azide-armed PSMA-617 scaffolds (**22-24**, not shown, prepared on solid phase) afforded **5-8** (see *below*).



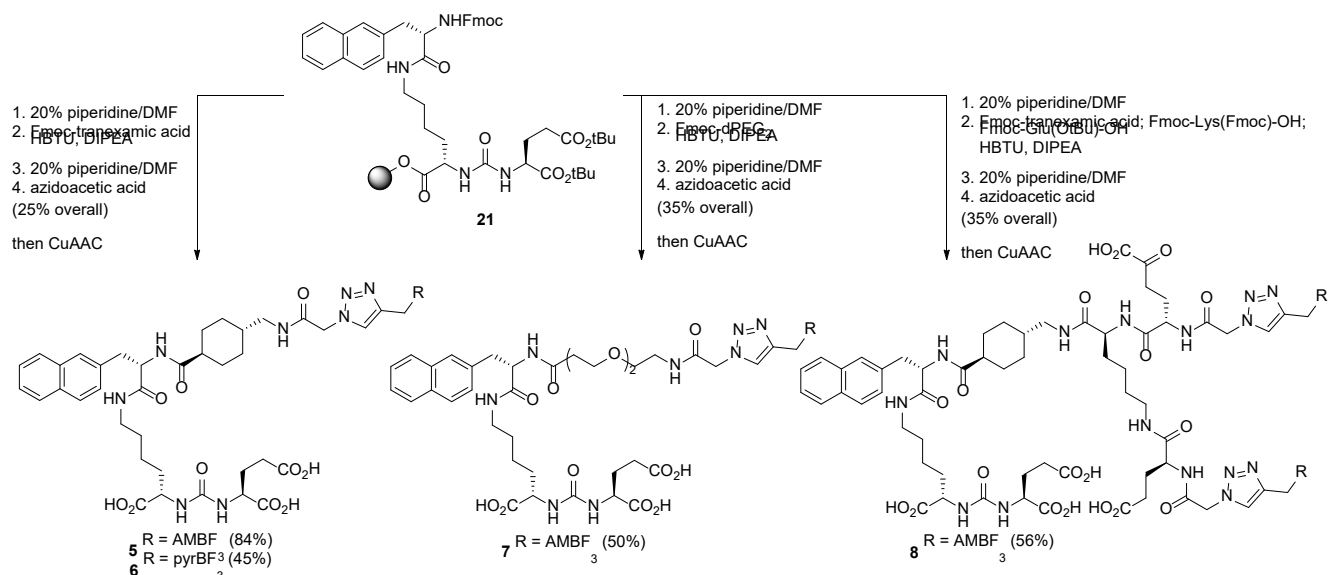
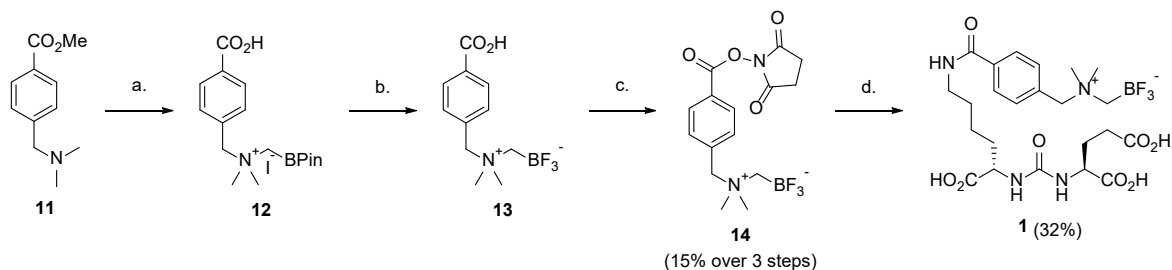


Figure S 2. General scheme for the synthesis of cold precursors 1–8.



**Conditions:** a. (Iodomethyl)boronic pinacol ester (1.4 eq.), THF, rt, 24h; b. KHF<sub>2</sub> (6 eq.), HCl (23 eq.), MeOH/water, 60°C, 72 h; c. *N*-hydroxysuccinimide (1.05 eq.), *N,N'*-diisopropylcarbodiimide (1.05 eq.), DMF, rt, 24h; d. Glu-ureido-Lys trifluoroacetate (1.67 eq.), diisopropylethylamine (24.5 eq.), MeOH, 50°C, 72 h.

### Synthesis of *N*-[4-(*N*-trifluoroborylmethyl-*N,N*-dimethylammoniomethyl)benzoyloxy]succinimide (**14**)

A solution of **11** (508 mg, 2.6 mmol) and (iodomethyl)boronic pinacol ester (1.0 g, 3.7 mmol) in distilled THF (10 mL) was stirred at room temperature for 24 h. The reaction mixture was concentrated under reduced pressure to obtain brown precipitant. The brown precipitant was washed with ether (10 mL × 5) and dried under vacuum. The crude intermediate **12** (1.4 g) and potassium hydrogen difluoride (1.2 g, 15.6 mmol) were dissolved in a mixture of H<sub>2</sub>O (8 mL) and MeOH (10 mL) in a 50-mL plastic falcon tube. HCl (5 mL, 12 M) was added to the solution. The reaction mixture was heated at 60 °C for 3 days. After being cooled to room temperature, the reaction mixture was filtered through a short path of silica gel, eluted with acetonitrile (100 mL), and concentrated to give viscous oil (720 mg). The viscous oil containing **13** was dissolved in DMF (10 mL). *N*-Hydroxysuccinimide (317 mg, 2.75 mmol) was added, followed by *N,N'*-diisopropylcarbodiimide (348 mg, 2.76 mmol). The reaction mixture was stirred at room temperature for 24 h. The reaction mixture was then concentrated under reduced pressure and purified by HPLC using the semi-preparative column eluted with 25 % acetonitrile in H<sub>2</sub>O at a flow rate of 4.5 mL/min and the retention time of the desired product was 10.6 min. The HPLC eluate

fractions containing the product were collected and lyophilized to yield compound **14** as white solid (150 mg, 15%).  $^1\text{H NMR}$  (300 MHz,  $\text{CDCl}_3$ ):  $\delta$  8.27 (d,  $J = 9.0$  Hz, 2H),  $\delta$  7.70 (d,  $J = 9.0$  Hz, 2H),  $\delta$  4.56 (s, 2H),  $\delta$  3.06 (s, 6H),  $\delta$  2.95 (s, 4H),  $\delta$  2.57 (m, 2H). MS (ESI): calculated for  $[\text{M} + \text{Na}]^+$   $\text{C}_{15}\text{H}_{18}\text{BF}_3\text{N}_2\text{NaO}_4$  358.1; observed 381.1.

### Synthesis of 1

Glu-ureido-Lys trifluoroacetate (38.8 mg, 0.122 mmol) and **14** (26 mg, 0.073 mmol) were dissolved in MeOH (3 mL) followed by *N,N*-diisopropylethylamine (312  $\mu\text{L}$ , 1.792 mmol). The reaction mixture was heated at 50  $^\circ\text{C}$  and stirred for 3 days and then concentrated under reduced pressure. The product was purified by HPLC using the semi-preparative column eluted with 15-35 % acetonitrile (0.5% acetic acid) in  $\text{H}_2\text{O}$  (0.5% acetic acid) at a flow rate of 4.5 mL/min. The HPLC eluate fractions containing the product were collected and lyophilized to yield **1** as a white solid (13 mg, 32%).  $^1\text{H NMR}$  (300 MHz,  $\text{D}_2\text{O}$ ):  $\delta$  7.77 (d,  $J = 9$  Hz, 2H),  $\delta$  7.60 (d,  $J = 9$  Hz, 2H),  $\delta$  4.42 (s, 2H),  $\delta$  4.15 (m, 3H),  $\delta$  3.36 (t,  $J = 6.0$ , 2H),  $\delta$  2.95 (s, 6H),  $\delta$  2.41 (t,  $J = 6.0$  Hz, 2H),  $\delta$  2.13-2.02 (m, 2H),  $\delta$  1.91-1.75 (m, 2H),  $\delta$  1.71-1.55 (m, 3H),  $\delta$  1.50-1.32 (m, 2H). MS (ESI): calculated for  $[\text{M} + \text{H}]^+$   $\text{C}_{23}\text{H}_{35}\text{BF}_3\text{N}_4\text{O}_8$  = 563.3; observed 563.4.

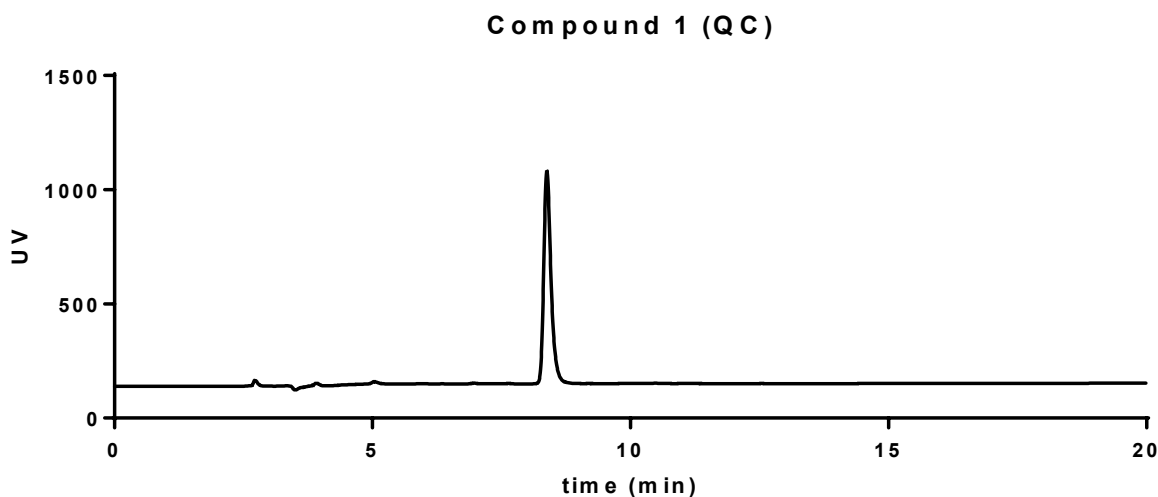
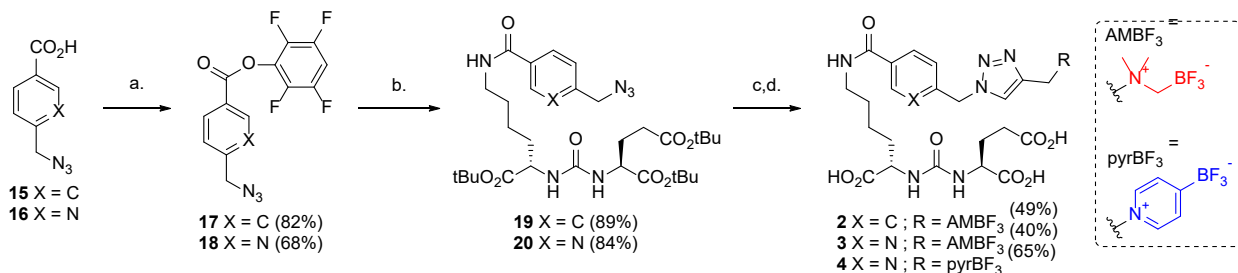


Figure S 3 - HPLC trace of pure **1**.



**Conditions:** a. 2,3,5,6-tetrafluorophenol (1.1 to 1.5 eq.), *N,N'*-dicyclohexylcarbodiimide (0.9 to 1.5 eq.),  $\text{CH}_2\text{Cl}_2$ , 0 $^\circ\text{C}$ , 3 h; b. *t*-butyl protected Glu-ureido-Lys (0.67 to 0.83 eq.), THF, rt, 16 h; c. 3% anisole in TFA, rt, 4 h; d. For **2** and **3**: *N*-propargyl-*N,N*-dimethyl-ammoniummethyltrifluoroborate (3 eq.),  $\text{CuSO}_4$  (3 eq.), Na ascorbate (6 eq.), MeCN/water, 45 $^\circ\text{C}$ , 2 h; For **4**: *N*-propargylpyridinium

*para*-trifluoroborate (0.4 eq., limiting reagent), CuSO<sub>4</sub> (0.18 eq.), Na ascorbate (0.36 eq.), NaHCO<sub>3</sub> (4 eq.), DMF/water, rt, 2 h.

### Synthesis of 2,3,5,6-tetrafluorophenyl 4-azidomethylbenzoate (**17**)

A solution of 4-(azidomethyl)benzoic acid **15** (719 mg, 4.0 mmol) and 2,3,5,6-tetrafluorophenol (731 mg, 4.4 mmol) in CH<sub>2</sub>Cl<sub>2</sub> (20 mL) was cooled in an ice/water bath. *N,N'*-dicyclohexylcarbodiimide (743 mg, 3.6 mmol) was added to the reaction mixture and stirred for 3 h. The reaction mixture was filtered and the filtrate was evaporated. After evaporation, the residue was dissolved in hexane (100 mL), and the solution was filtered again and washed with 1N NaOH aqueous solution (100 mL). The organic phase was dried over anhydrous magnesium sulfate, concentrated under reduced pressure, and purified by chromatography on silica gel eluted with 1:5 ether/hexane to obtain the desired product **17** as white solid (1.06 g, 82%). <sup>1</sup>H NMR (300 MHz, CDCl<sub>3</sub>): δ 8.25 (d, *J* = 9 Hz, 2H), δ 7.52 (d, *J* = 9 Hz, 2H), δ 7.06 (m, 1H), δ 4.42 (s, 2H), δ 4.15 (m, *J* = 4.9, 2H), δ 3.36 (t, *J* = 6.0 Hz, 2H), δ 2.95 (s, 6H), δ 2.41 (t, *J* = 6.0 Hz, 2H), δ 4.50 (s, 2H). MS (ESI): calculated for [M]<sup>-</sup> C<sub>14</sub>H<sub>7</sub>F<sub>4</sub>N<sub>3</sub>O<sub>2</sub> 325.1; observed 325.6.

### Synthesis of (S)-2-[3-[5-(4-azidomethylbenzoylamino)-(S)-1-(*tert*-butoxyloxycarbonyl)pentyl]ureido] pentanedioic acid bis(4-*tert*-butyl) ester (**19**)

A solution of *t*-butyl protected Glu-ureido-Lys (101.9 mg, 0.21 mmol) and **17** (100.1 mg, 0.31 mmol) in THF (20 mL) was stirred overnight at room temperature. The reaction mixture was concentrated under reduced pressure and purified by chromatography on silica gel eluted with 1:1 hexane/EtOAc to obtain the desired product **19** as a light-yellow oil (120.6 mg, 89%). <sup>1</sup>H NMR (300 MHz, CDCl<sub>3</sub>): δ 7.89 (d, *J* = 8.2 Hz 2H), δ 7.37 (d, *J* = 8.2 Hz, 2H), δ 7.05 (bt, 1H), δ 5.43 (m, 1H), δ 5.33 (m, 1H), δ 4.39 (s, 2H), δ 4.25 (m, 2H), δ 3.53-3.36 (m, 2H), δ 2.28 (m, 2H), δ 2.10-1.96 (m, 1H), δ 1.87-1.75 (m, 2H), δ 1.69-1.56 (m, 3H), δ 1.43 (s, 18H), δ 1.40 (s, 9H). MS (ESI): calculated for [M + H]<sup>+</sup> C<sub>32</sub>H<sub>51</sub>N<sub>6</sub>O<sub>8</sub> 647.4; observed 647.6.

### Synthesis of **2**

A solution of **19** (98 mg, 0.15 mmol) in TFA (5 mL) containing 3% anisole was stirred at room temperature. After 4 h, the reaction mixture was concentrated under reduced pressure. The residue was dissolved in water (1 mL) and wash with hexane (1 mL × 3) to remove anisole. The aqueous phase was lyophilized to obtain a yellow oil. The crude product was purified by HPLC using the semi-preparative column eluted with 25-50 % acetonitrile (0.1% TFA) in water (0.1% TFA) in 25 min at a flow rate of 4.5 mL/min, and the retention time of the desired product was 10 min. The HPLC eluate fractions containing the product were collected and lyophilized to yield **deprotected 19** as white solid (71 mg, 99%). <sup>1</sup>H NMR (300 MHz, D<sub>2</sub>O): δ 7.72 (d, *J* = 8.2 Hz 2H), δ 7.47 (d, *J* = 8.2 Hz, 2H), δ 4.65-4.90 (m, 2H), δ 4.46 (s, 2H), δ 4.16 (dd, *J* = 4.9, 8.8 Hz, 2H), δ 3.37 (t, *J* = 6.8 Hz, 2H), δ 2.43 (t, *J* = 7.4 Hz, 2H), δ 2.10-2.15 (m, 1H), δ 1.75-1.60 (m, 3H), δ 1.47-1.43 (m, 2H). MS (ESI): calculated for [M + H]<sup>+</sup> C<sub>20</sub>H<sub>27</sub>N<sub>6</sub>O<sub>8</sub> 479.2; observed 479.3.

A solution of **deprotected 19** (10.5 mg, 0.022 mmol), *N*-propargyl-*N,N*-dimethylammoniumtrifluoroborate (10.7 mg, 0.065 mmol), 1 M CuSO<sub>4</sub> (65 μL), and 1 M sodium ascorbate (162.5 μL) in acetonitrile (150 μL) was incubated at 45 °C for 2 h. The reaction mixture was purified by HPLC using the semi-preparative column eluted with 15-35 % acetonitrile (0.5 % acetic acid) in water (0.5 % acetic acid) at a flow rate of 4.5 mL/min. The HPLC eluate fractions containing the product were collected and lyophilized to yield **2** as white solid (7 mg, 49 %). <sup>1</sup>H

NMR (300 MHz, D<sub>2</sub>O):  $\delta$  8.31 (s, 1H),  $\delta$  7.69 (d,  $J$  = 9 Hz, 2H),  $\delta$  7.38 (d,  $J$  = 9 Hz, 2H),  $\delta$  5.69 (s, 2H),  $\delta$  4.72 (s, 2H),  $\delta$  4.03 (m, 2H),  $\delta$  3.33 (m, 2H),  $\delta$  3.13 (m, 1H),  $\delta$  2.97 (s, 6H),  $\delta$  2.40-2.32 (m, 3H),  $\delta$  1.99 (m, 2H),  $\delta$  1.88-1.69 (m, 2H),  $\delta$  1.67-1.50 (m, 2H),  $\delta$  1.45-1.30 (m, 2H). MS (ESI): calculated for [M + H]<sup>+</sup> C<sub>26</sub>H<sub>38</sub>BF<sub>3</sub>N<sub>7</sub>O<sub>8</sub> 644.3; observed 644.4

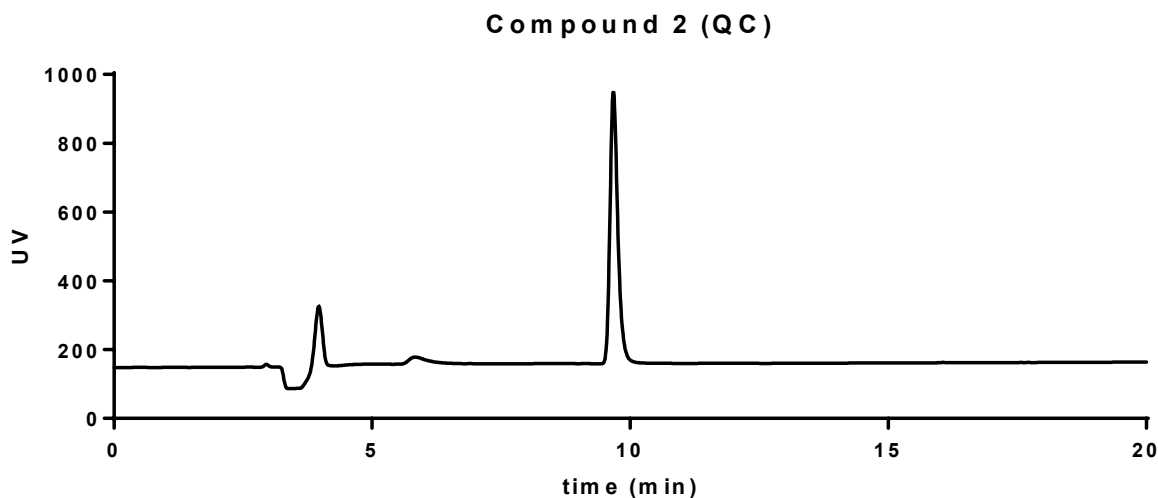


Figure S 4 - HPLC trace of pure **2**.

#### Synthesis of 2,3,5,6-tetrafluorophenyl 4-azidomethylnicotinate (**18**)

A solution of 6-(azidomethyl)nicotinic acid **16** (507 mg, 2.8 mmol) and 2,3,5,6-tetrafluorophenol (700 mg, 4.2 mmol) in CH<sub>2</sub>Cl<sub>2</sub> (20 mL) was cooled in an ice/water bath. *N,N'*-dicyclohexylcarbodiimide (865 mg, 4.2 mmol) was added to the reaction mixture and stirred for 3 h. The reaction mixture was filtered and the filtrate was concentrated under reduced pressure, and purified by chromatography on silica gel eluted with 1:30 ether/hexane to obtain the desired product **2** as white solid (626.7 mg, 68%). <sup>1</sup>H NMR (300 MHz, CDCl<sub>3</sub>):  $\delta$  9.36 (d,  $J$  = 2.2 Hz, 1H),  $\delta$  8.49 (dd,  $J$  = 8.0, 2.2 Hz, 1H),  $\delta$  7.57 (d,  $J$  = 8.0 Hz, 1H),  $\delta$  7.08 (m, 1H),  $\delta$  4.64 (s, 2H) MS (ESI): calculated for C<sub>13</sub>H<sub>6</sub>F<sub>4</sub>N<sub>4</sub>O<sub>2</sub> [M + H]<sup>+</sup> = 327.05; observed [M + H]<sup>+</sup> = 327.30.

#### Synthesis of (S)-2-[3-[5-(4-azidomethylpicolylamino)-(S)-1-(tert-butoxyloxycarbonyl)pentyl]ureido] pentanedioic acid bis(4-tert-butyl) ester (**20**)

A solution of *t*-butyl protected Glu-ureido-Lys (141.1 mg, 0.30 mmol) and **18** (118.0 mg, 0.36 mmol) in THF (20 mL) was stirred overnight at room temperature. The reaction mixture was concentrated under reduced pressure and purified by chromatography on silica gel eluted with 2:3 hexane/EtOAc to obtain the desired product **20** as light yellow oil (163.2 mg, 84%). <sup>1</sup>H NMR (300 MHz, CDCl<sub>3</sub>):  $\delta$  9.09 (d,  $J$  = 1.9 Hz 1H),  $\delta$  8.26 (dd,  $J$  = 8.3, 2.2 Hz 1H),  $\delta$  7.45 (bt, 1H),  $\delta$  7.43 (d,  $J$  = 8.3 Hz, 1H),  $\delta$  5.50 (d,  $J$  = 7.7 Hz 1H),  $\delta$  5.32 (d,  $J$  = 8.0 Hz 1H),  $\delta$  4.53 (s, 2H),  $\delta$  4.23 (m, 2H),  $\delta$  3.57-3.38 (m, 2H),  $\delta$  2.29 (m, 2H),  $\delta$  2.20-1.97 (m, 1H),  $\delta$  1.82-1.76 (m, 2H),  $\delta$  1.68-1.56 (m, 3H),  $\delta$  1.43 (s, 18H),  $\delta$  1.38 (s, 9H). MS (ESI): calculated for C<sub>31</sub>H<sub>49</sub>N<sub>7</sub>O<sub>8</sub> [M + H]<sup>+</sup> = 648.37; observed [M + H]<sup>+</sup> = 648.60.

### Synthesis of 3

A solution of **20** (163.2 mg, 0.15 mmol) in TFA (5 mL) containing 3% anisole was stirred at room temperature. After 4 h, the reaction mixture was concentrated under reduced pressure. The residue was dissolved in water (2 mL) and wash with hexane (2 mL × 3) to remove anisole. The aqueous phase was lyophilized to obtain crude a yellow oil (180.2 mg). The crude product (20.0 mg, 0.04 mmol), *N*-propargyl-*N,N*-dimethyl-ammoniomethyltrifluoroborate (20.6 mg, 0.13 mmol), 1 M CuSO<sub>4</sub> (124 μL), and 1 M sodium ascorbate (310 μL) in acetonitrile (150 μL) and 5 % NH<sub>4</sub>OH (300 μL) was incubated at 45 °C for 2 h. The reaction mixture was purified by HPLC using semi-preparative column eluted with 3-13 % acetonitrile in ammonium formate buffer (40 mM, pH 6.0) at a flow rate of 4.5 mL/min. **3** was obtained as white solid (10.4 mg, 40 %). MS (ESI): calculated for C<sub>25</sub>H<sub>36</sub>BF<sub>3</sub>N<sub>8</sub>O<sub>8</sub> [M + H]<sup>+</sup> = 645.28; observed [M + H]<sup>+</sup> = 645.50.

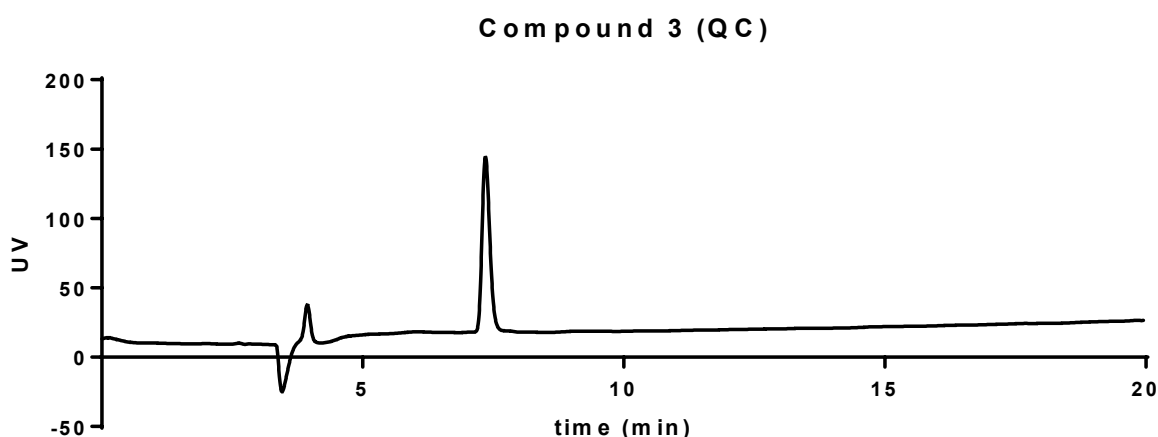
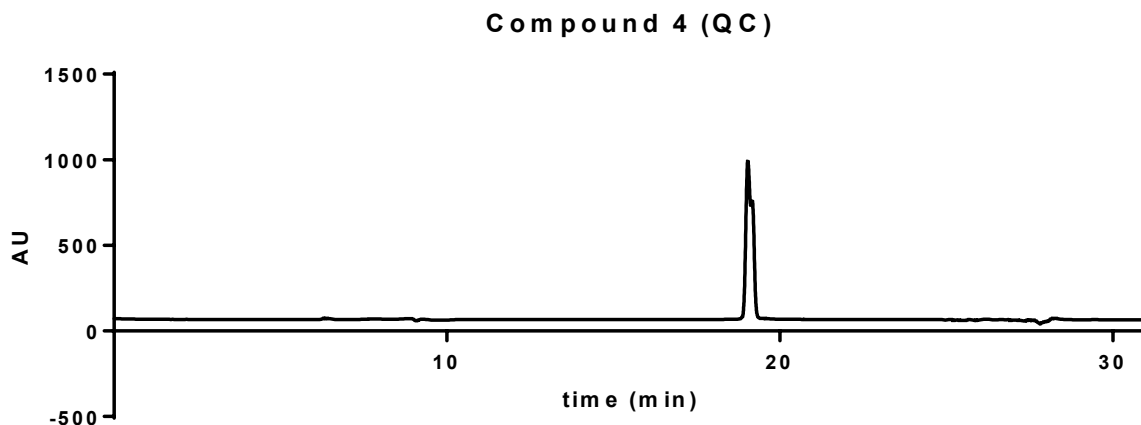
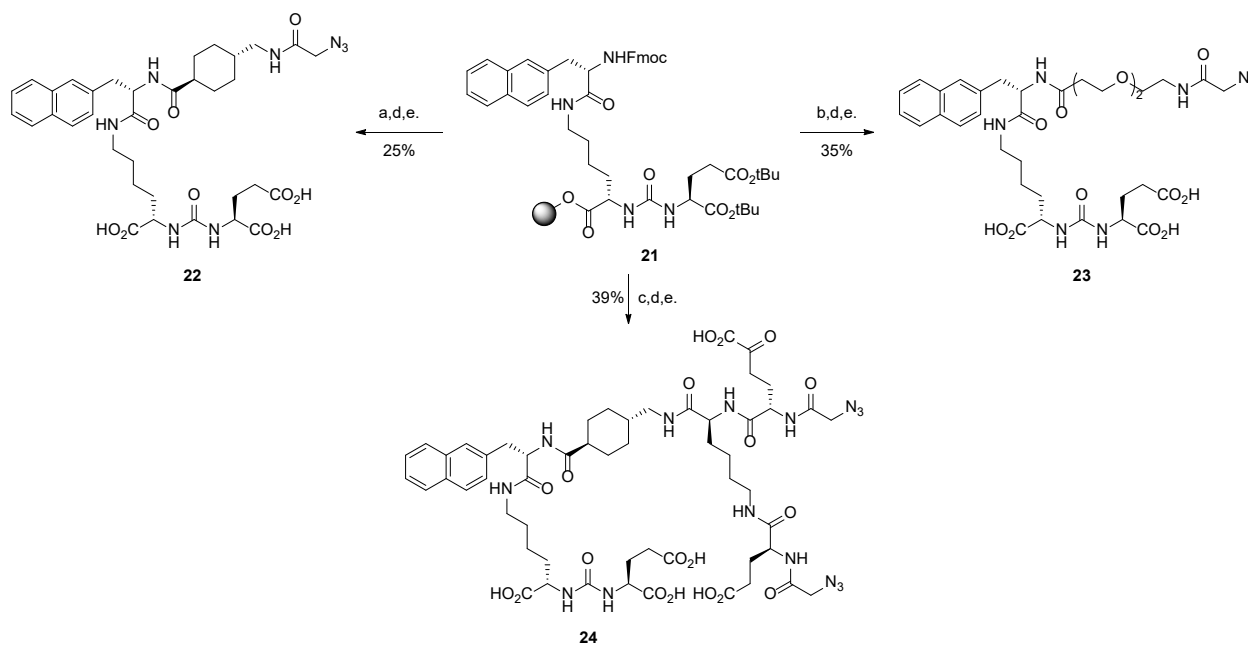


Figure S 5 - HPLC trace of pure **3**.

### Synthesis of 4

To a solution of *N*-propargylpyridinium *para*-trifluoroborate (1 eq., 2.6 mg, 14 μmol) and deprotected **20** (2.5 eq., 16.8 mg, 35 μmol) in DMF (500 μL) at room temperature was added a bright yellow solution of Cu<sup>(II)</sup> prepared by mixing 0.1M aq. CuSO<sub>4</sub> (10 mol%, 14 μL, 1.4 μmol), 0.2M aq. sodium ascorbate (20 mol%, 14 μL, 2.8 μmol) and 1M aq. sodium bicarbonate (1 eq., 14 μL, 14 μmol) with H<sub>2</sub>O (58 μL). The mixture was stirred at room temperature for 2h, but low conversion was assessed by TLC. An excess of 1M aq. sodium bicarbonate (10 eq., 141 μL, 141 μmol) was added, causing a gas release. To ensure reaction rate, another portion of 0.1 M aq. CuSO<sub>4</sub> (35 mol%, 49 μL, 4.9 μmol) and 0.2M aq. sodium ascorbate (70 mol%, 49 μL, 98 μmol) were added. The mixture was stirred at room temperature for 5 min. The reaction was then quenched with 10 drops of ammonia and then filtered through a small silica gel pad (2 cm high, 0.5 cm) built in a Pasteur pipet, eluting with a 9.5/9.5/1 mixture of MeCN/MeOH/ammonium hydroxide (10 mL). The filtrate was concentrated, then diluted with water (4 mL), frozen and lyophilized. The dry residue was purified by HPLC using semi-preparative column eluted with 0-30 % acetonitrile (0.1% formic acid) in water 0.1% formic acid) at a flow rate of 2 mL/min (retention time = 19.0 min) to afford pure **4** (6.1 mg, 65% yield). ESI-HRMS (TOF) *m/z* [M-H]<sup>-</sup> 662.2352; calc. 662.2346 for C<sub>27</sub>H<sub>31</sub>N<sub>8</sub>O<sub>8</sub><sup>10</sup>BF<sub>3</sub>.

Figure S 6 - HPLC trace of pure **4**.

**Conditions:** a. (i) 20% piperidine/DMF (v/v), rt, 30 min; (ii) Fmoc-tranexamic acid, HBTU, DIPEA, rt, 2 h; b. (i) 20% piperidine/DMF (v/v), rt, 30 min; (ii) Fmoc-dPEG2, HBTU, DIPEA, rt, 2 h; c. (i) 20% piperidine/DMF (v/v), rt, 30 min; (ii) Fmoc-dPEG2; Fmoc-Lys(Fmoc)-OH; Fmoc-Glu(OtBu)-OH, HBTU, DIPEA, rt, 2 h; d. (i) 20% piperidine/DMF (v/v), rt, 30 min; (ii) azidoacetic acid (5 eq.), DCC (5 eq.), NHS (6 eq.), rt, 2 h; e. TFA/TIS 95:5 (v/v), rt, 2 h.

### Synthesis of **21**

Resin-bound **21** was synthesized on solid phase by following reported procedures.<sup>(8)</sup>

### Synthesis of **22**

After Fmoc deprotection of **21**, Fmoc-protected tranexamic acid was coupled to the *N*-terminus according to a reported procedure.<sup>(8)</sup> After Fmoc deprotection, 2-azidoacetic acid (5 equivalents)

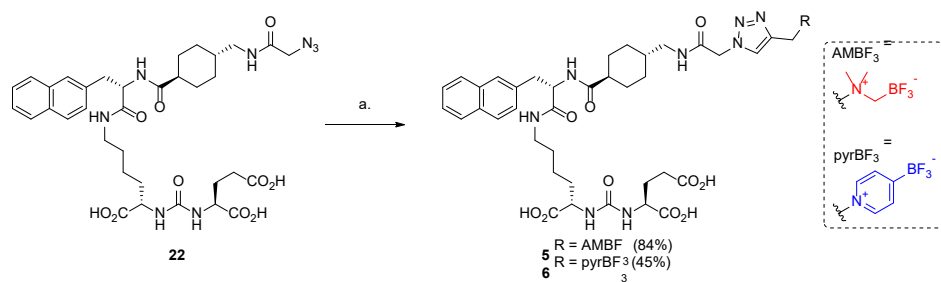
was coupled to the *N*-terminus using the *in situ* activating reagent *N,N'*-diisopropylcarbodiimide (5 eq.) and *N*-hydroxysuccinimide (6 eq.) in DMF for 2 h at room temperature. At the end, the peptide was deprotected and simultaneously cleaved from the resin by treating the beads with a TFA/TIS 95:5 (v/v) mixture for 2 h at room temperature. After filtration, the peptide was precipitated by the addition of cold diethyl ether to the TFA solution. The crude peptide was purified by HPLC using a semi-preparative column eluted with 35-45 % acetonitrile (0.1% TFA) in water (0.1% TFA) at a flow rate of 4.5 mL/min. Collection of the peak with a retention time of 9.1 min afforded **22** in 25 % yield. MS (ESI): calculated for C<sub>35</sub>H<sub>46</sub>N<sub>8</sub>O<sub>10</sub> [M + H]<sup>+</sup> = 739.80; observed [M + H]<sup>+</sup> = 740.26.

### Synthesis of 23

After Fmoc deprotection of **21**, Fmoc-protected dPEG<sub>2</sub> acid was coupled to the *N*-terminus using standard solid-phase peptide synthesis. The Fmoc protecting group was removed and 2-azidoacetic acid (5 equivalents) was coupled to the *N*-terminus with the *in situ* activating reagent *N,N'*-diisopropylcarbodiimide (5 equivalents) and *N*-hydroxysuccinimide (6 equivalents) in DMF for 2 h at room temperature. At the end, the peptide was deprotected and simultaneously cleaved from the resin by treating with 95/5 TFA/TIS for 2 h at room temperature. After filtration, the peptide was precipitated by the addition of cold diethyl ether to the TFA solution. The crude peptide was purified by HPLC using the semi-preparative column eluted with 31-40 % acetonitrile (0.1% TFA) in water at a flow rate of 4.5 mL/min. The retention time was 9.8 min, and the yield of the peptide **23** was 35.5 %. MS (ESI): calculated for C<sub>34</sub>H<sub>46</sub>N<sub>8</sub>O<sub>12</sub> [M + H]<sup>+</sup> = 759.33; observed [M + H]<sup>+</sup> = 759.50.

### Synthesis of 24

After Fmoc deprotection of **21**, Fmoc-protected tranexamic acid was coupled to the *N*-terminus followed by Fmoc-Lys(Fmoc)-OH and Fmoc-Glu(OtBu)-OH via solid-phase peptide synthesis using Fmoc-based chemistry. After Fmoc deprotection, 2-azidoacetic acid (5 equivalents) was coupled to the *N*-terminus using the *in situ* activating reagent *N,N'*-diisopropylcarbodiimide (5 eq.) and *N*-hydroxysuccinimide (6 eq.) in DMF for 2 h at room temperature. At the end, the peptide was deprotected and simultaneously cleaved from the resin by treating the beads with a TFA/TIS 95:5 (v/v) mixture for 2 h at room temperature. After filtration, the peptide was precipitated by the addition of cold diethyl ether to the TFA solution. The crude peptide was purified by HPLC using a semi-preparative column eluted with 33 % acetonitrile (0.1% TFA) in water (0.1% TFA) at a flow rate of 4.5 mL/min. Collection of the peak with a retention time of 10.1 min afforded **22** in 39 % yield. MS (ESI): calculated for C<sub>53</sub>H<sub>73</sub>N<sub>15</sub>O<sub>18</sub> [M + H]<sup>+</sup> = 1208.53; observed [M + H]<sup>+</sup> = 1208.68.



**Conditions:** a.  $\text{AMBF}_3$  or  $\text{pyrBF}_3$  (2–5 eq.),  $\text{CuSO}_4$  (cat.), Na ascorbate (cat.),  $\text{NH}_4\text{OH}$ ,  $\text{MeCN}/\text{H}_2\text{O}$ ,  $45^\circ\text{C}$ , 2 h.

### Synthesis of 5

A solution of **22** (3.8 mg,  $5\ \mu\text{mol}$ ), *N*-propargyl-*N,N*-dimethyl-ammoniumtrifluoroborate (4 mg,  $24.2\ \mu\text{mol}$ ), 1 M  $\text{CuSO}_4$  (25  $\mu\text{L}$ ), and 1 M sodium ascorbate (70  $\mu\text{L}$ ) in acetonitrile (150  $\mu\text{L}$ ) and 5 %  $\text{NH}_4\text{OH}$  (150  $\mu\text{L}$ ) was incubated at  $45^\circ\text{C}$  oil bath for 2 h. The reaction mixture was purified by HPLC using the semi-preparative column eluted with 21 % acetonitrile and 79 % ammonia formate buffer (40 mM, pH 6.0) at a flow rate of 4.5 mL/min. The yield of the peptide was 84 %. MS (ESI): calculated for  $\text{C}_{41}\text{H}_{57}\text{BF}_3\text{N}_9\text{O}_{10}$   $[\text{M} + \text{H}]^+ = 904.44$ ; observed  $[\text{M} + \text{H}]^+ = 904.60$ .

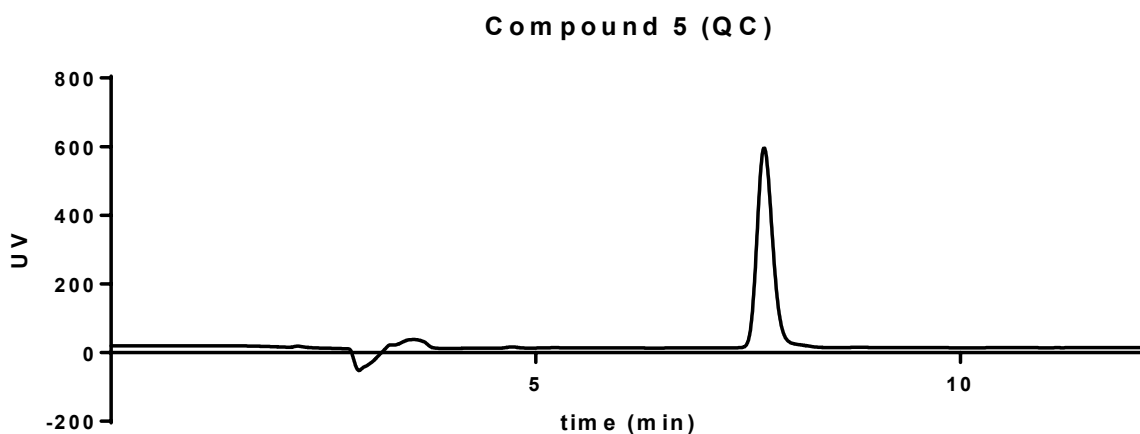
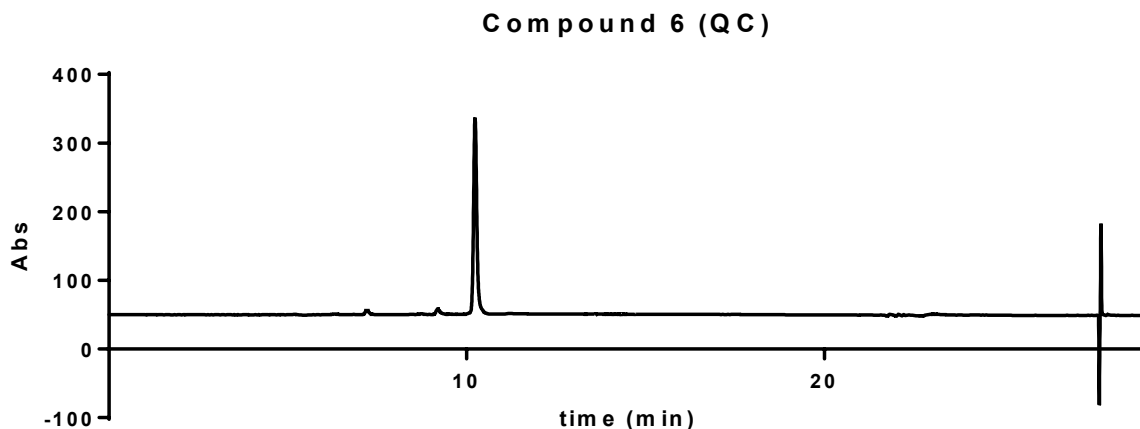
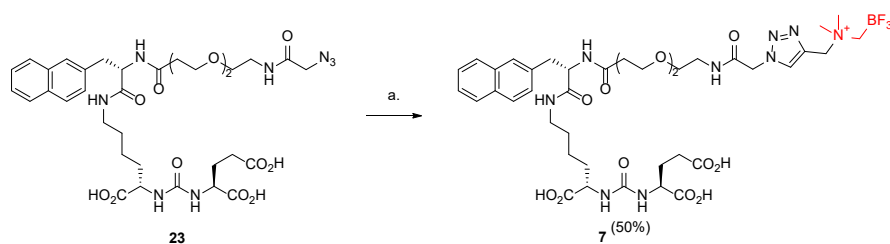


Figure S 7 - HPLC trace of pure **5**.

### Synthesis of 6

A solution of **22** (2.5 mg,  $3.4\ \mu\text{mol}$ ), *N*-propargyl-*para*-pyridiniumtrifluoroborate (1.3 mg,  $6.8\ \mu\text{mol}$ ), 1 M  $\text{CuSO}_4$  (25  $\mu\text{L}$ ), and 1 M sodium ascorbate (70  $\mu\text{L}$ ) in acetonitrile (150  $\mu\text{L}$ ) and 5 %  $\text{NH}_4\text{OH}$  (150  $\mu\text{L}$ ) was incubated at  $45^\circ\text{C}$  oil bath for 2 h. The reaction mixture was purified by HPLC using the semi-preparative column eluted with a gradient of acetonitrile and formate buffer (40 mM, pH 6.0) at a flow rate of 2 mL/min to afford the peptide with 45 % yield. ESI-HRMS (TOF)  $m/z$   $[\text{M}-\text{H}]^-$  921.3918; calc. 921.3919 for  $\text{C}_{43}\text{H}_{52}\text{BF}_3\text{N}_9\text{O}_{10}$ .

Figure S 8 - HPLC trace of pure **6**.

**Conditions:** a. AMBF<sub>3</sub> or pyrBF<sub>3</sub> (3.5 eq.), CuSO<sub>4</sub> (cat.), Na ascorbate (cat.), NH<sub>4</sub>OH, MeCN/H<sub>2</sub>O, 45°C, 2 h.

### Synthesis of **7**

A solution of **23** (10.5 mg, 0.014 mmol), *N*-propargyl-*N,N*-dimethyl-ammoniumtrifluoroborate (8.0 mg, 48.6 μmol), 1 M CuSO<sub>4</sub> (30 μL), and 1 M sodium ascorbate (72 μL) in acetonitrile (100 μL) and 5 % NH<sub>4</sub>OH (100 μL) was incubated at 45 °C oil bath for 2 h. The reaction mixture was purified by HPLC using the semi-preparative column eluted with 20 % acetonitrile and 80 % ammonia formate buffer (40 mM, pH 6.0) at a flow rate of 4.5 mL/min. The yield of the peptide was 50.0 %. MS (ESI): calculated for C<sub>40</sub>H<sub>57</sub>BF<sub>3</sub>N<sub>9</sub>O<sub>12</sub> [M + Na]<sup>+</sup> = 946.41; observed [M + Na]<sup>+</sup> = 946.60.

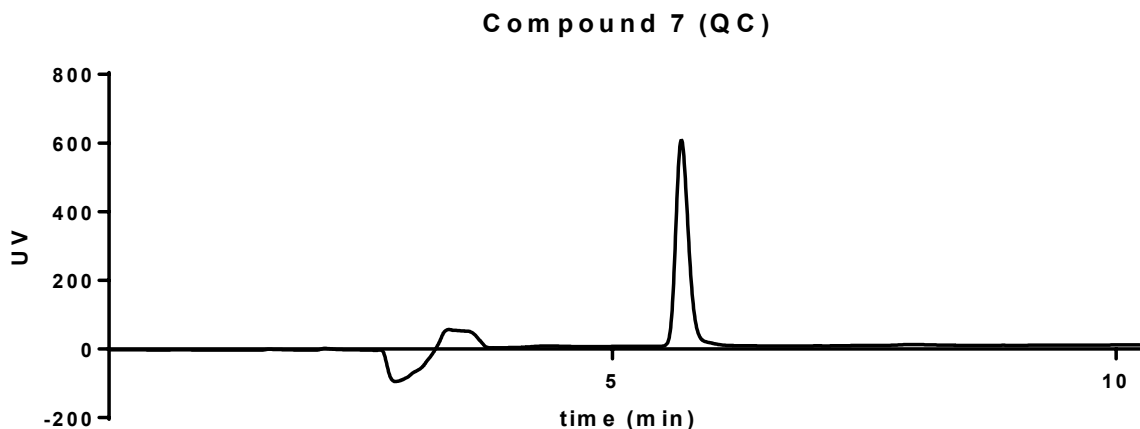
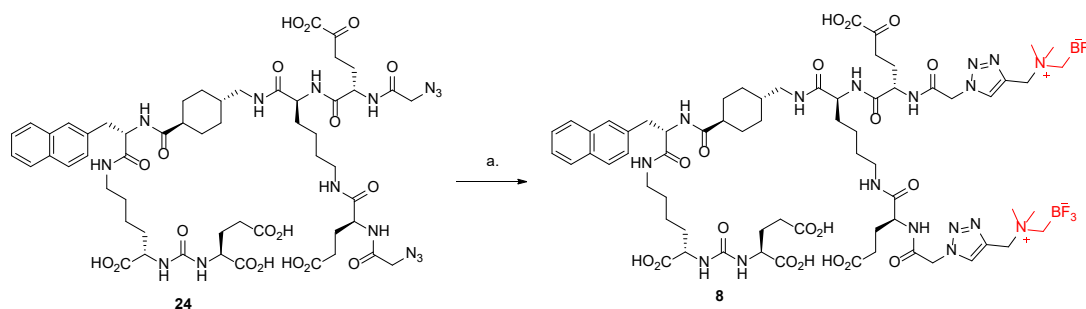


Figure S 9 - HPLC trace of pure 7.



**Conditions:** a. AMBF<sub>3</sub> (6 eq.), CuSO<sub>4</sub> (cat.), Na ascorbate (cat.), NH<sub>4</sub>OH, MeCN/H<sub>2</sub>O, 45°C, 2 h.

### Synthesis of 8

A solution of **24** (6.0 mg, 5.0 μmol), *N*-propargyl-*N,N*-dimethyl-ammoniumethyltrifluoroborate (4.9 mg, 30.0 μmol), 1 M CuSO<sub>4</sub> (37.5 μL), and 1 M sodium ascorbate (94 μL) in acetonitrile (150 μL) and 5 % NH<sub>4</sub>OH (150 μL) was incubated at 45 °C oil bath for 2 h. The reaction mixture was purified by HPLC using the semi-preparative column eluted with 15 % acetonitrile and 85 % ammonia formate buffer (40 mM, pH 6.0) at a flow rate of 4.5 mL/min. The yield of the peptide was 56.0 %. MS (ESI): calculated for C<sub>65</sub>H<sub>95</sub>B<sub>2</sub>F<sub>6</sub>N<sub>17</sub>O<sub>18</sub> [M + H]<sup>+</sup> = 1538.72; observed [M + H]<sup>+</sup> = 1538.88.

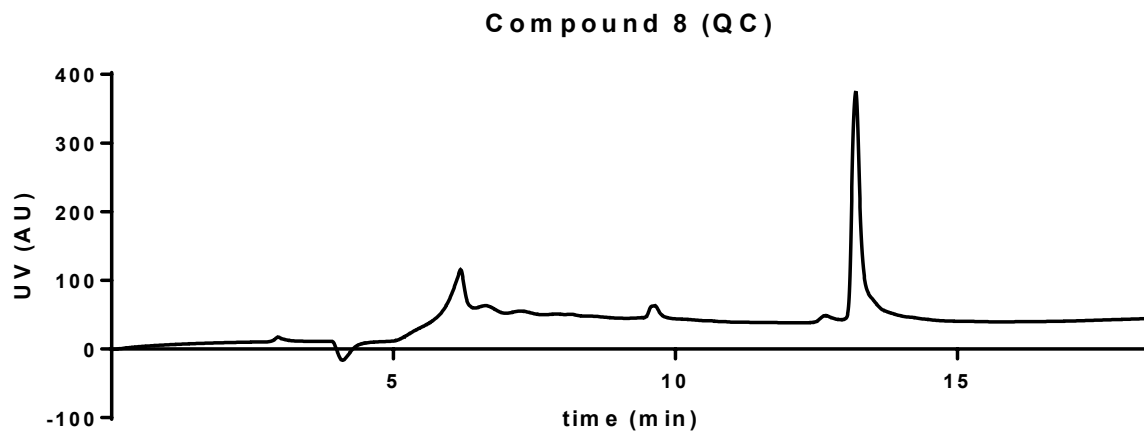


Figure S 10 – HPLC trace of pure **8**.

QC ANALYSIS OF TRACERS [ $^{18}\text{F}$ ]1-8

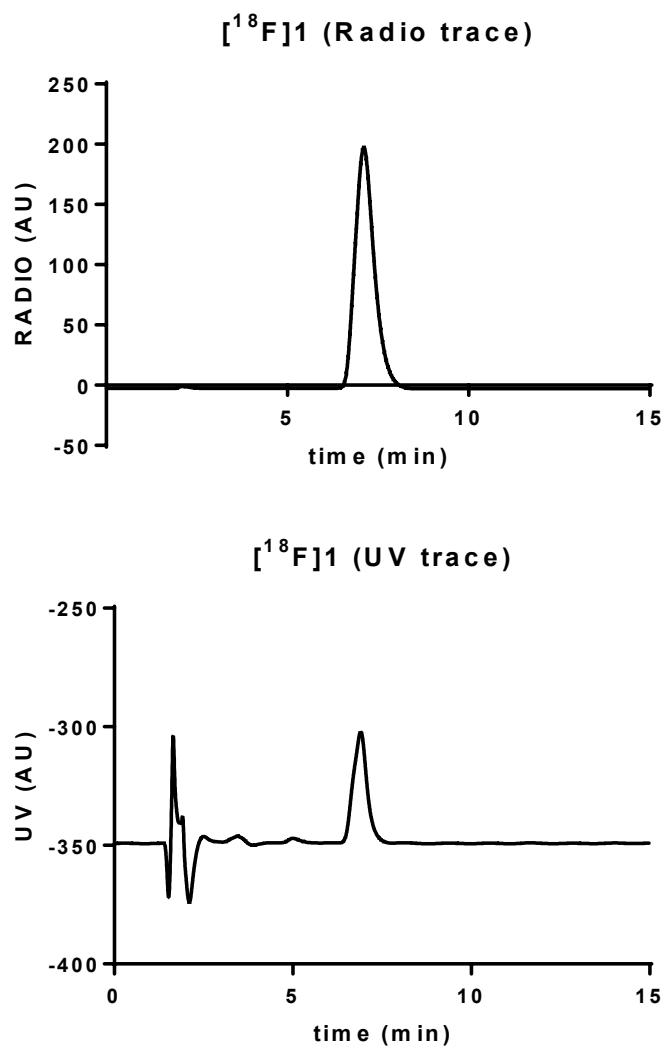


Figure S 11 - QC analysis of [ $^{18}\text{F}$ ]1.

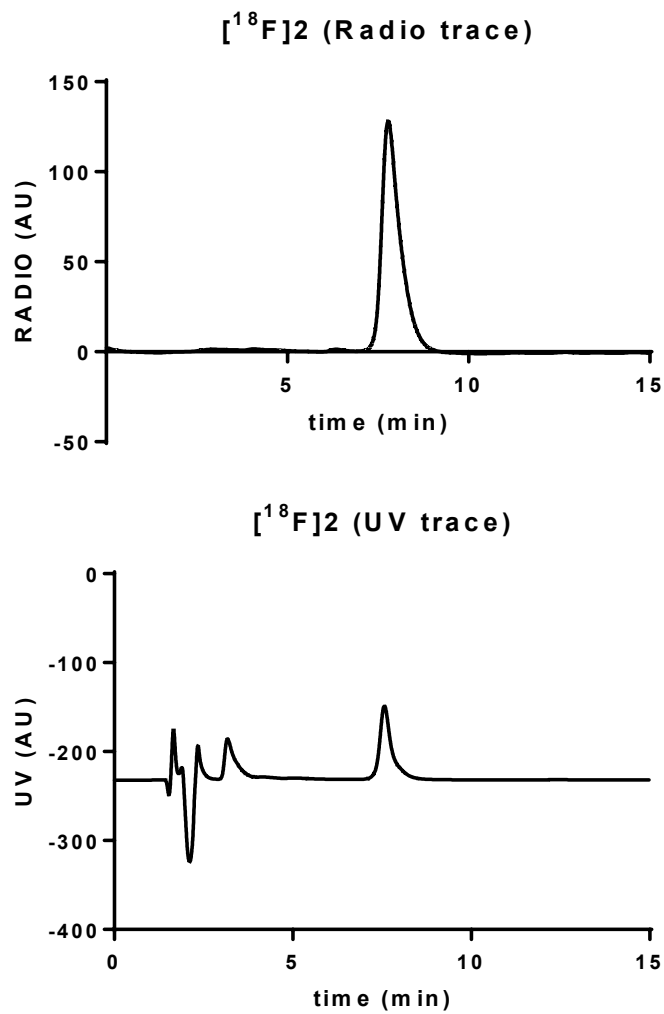


Figure S 12 - QC analysis of [<sup>18</sup>F]2.

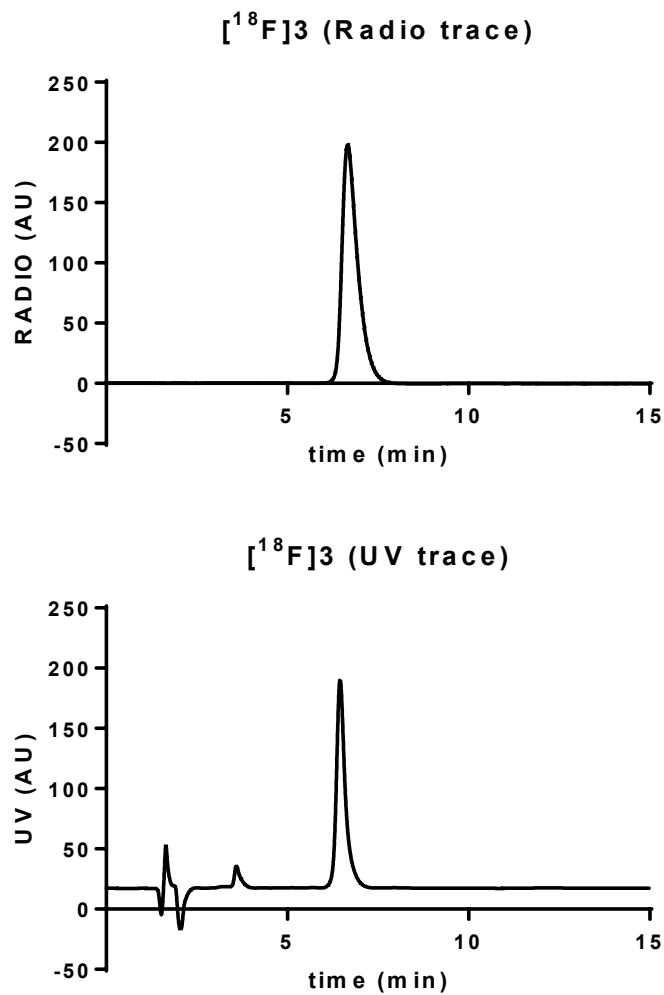


Figure S 13 - QC analysis of [<sup>18</sup>F]3.

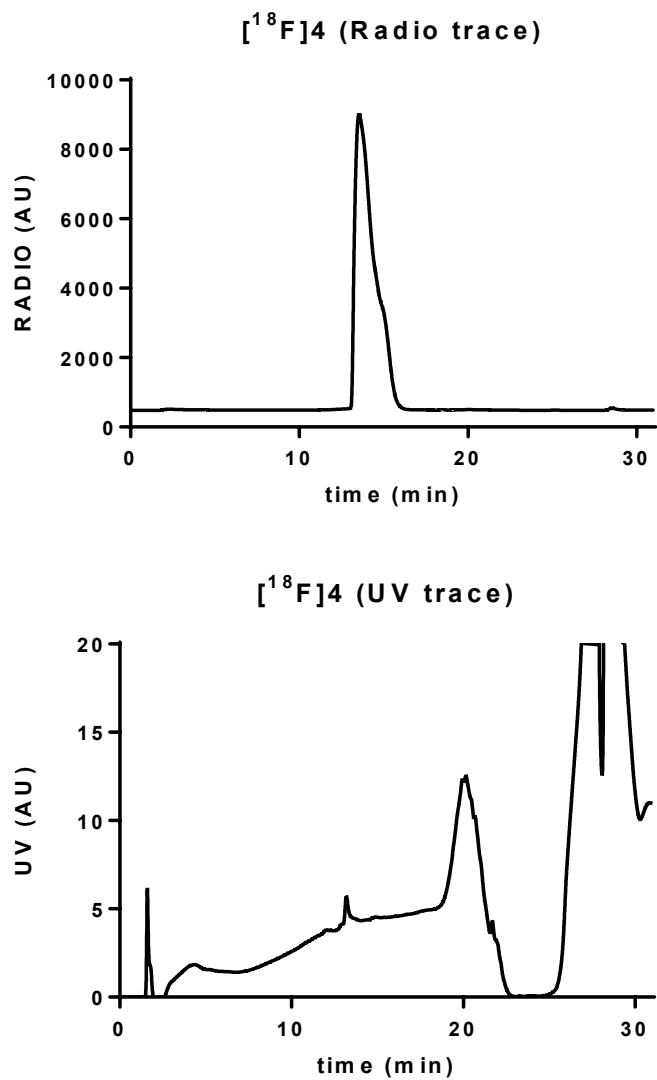


Figure S 14 - QC analysis of [<sup>18</sup>F]4.

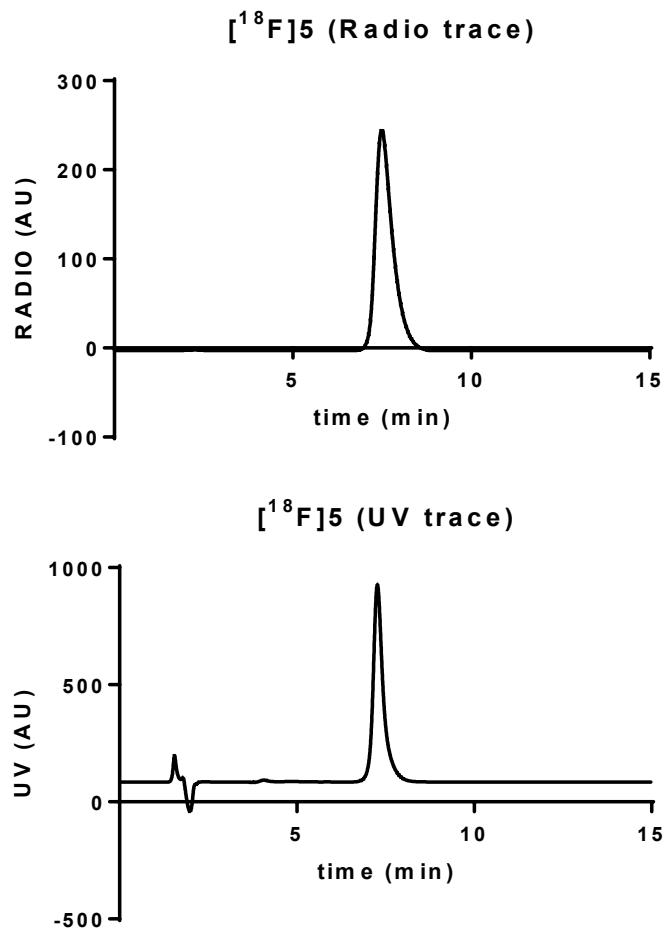


Figure S 15 - QC analysis of [<sup>18</sup>F]5.

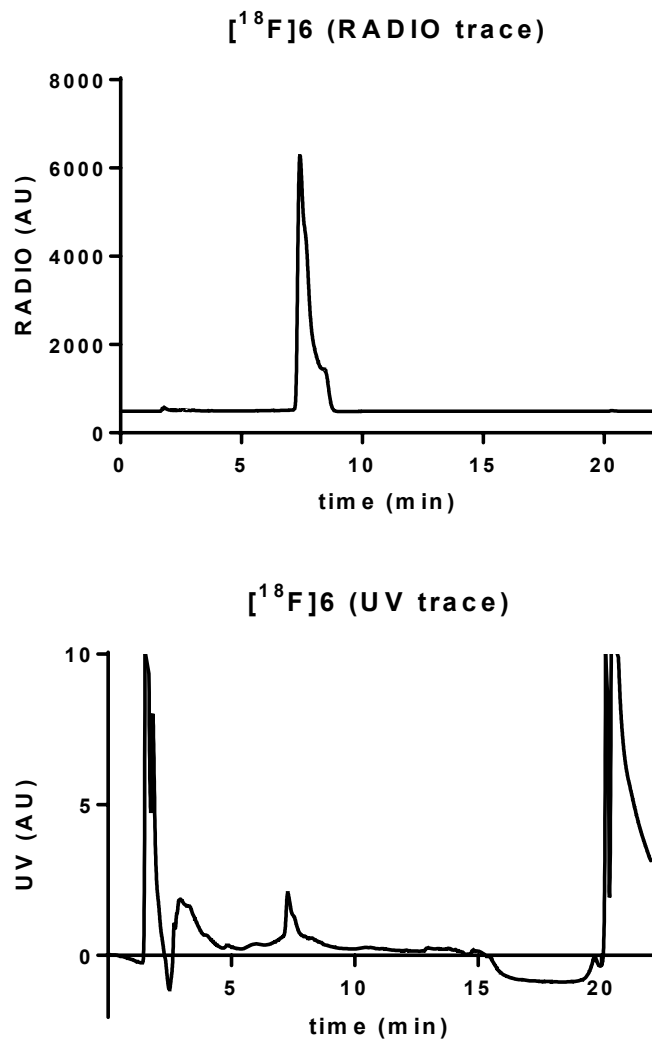


Figure S 16 - QC analysis of [<sup>18</sup>F]6.

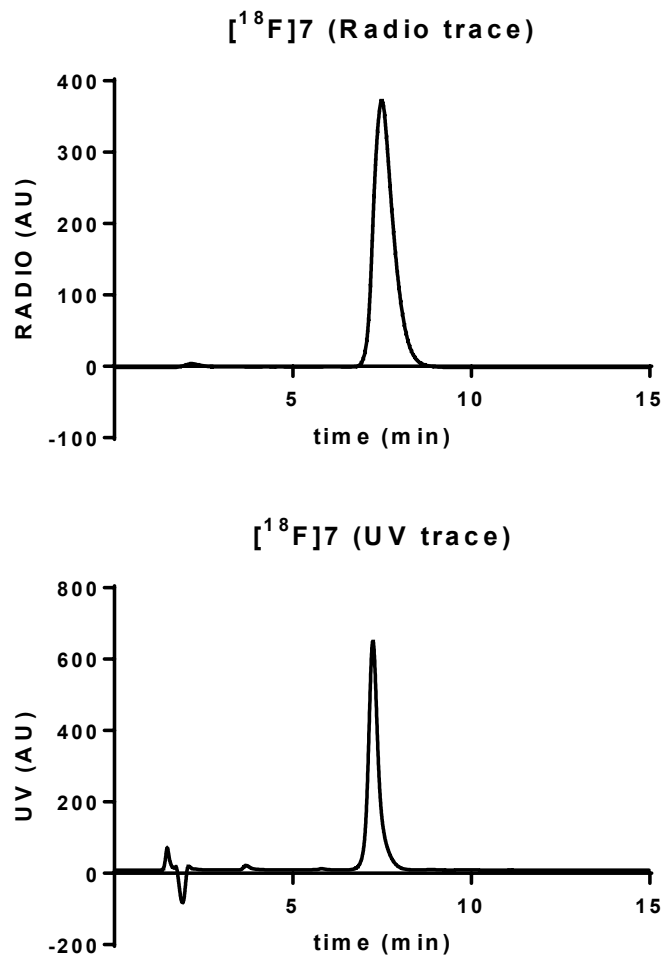


Figure S 17 - QC analysis of [<sup>18</sup>F]7.

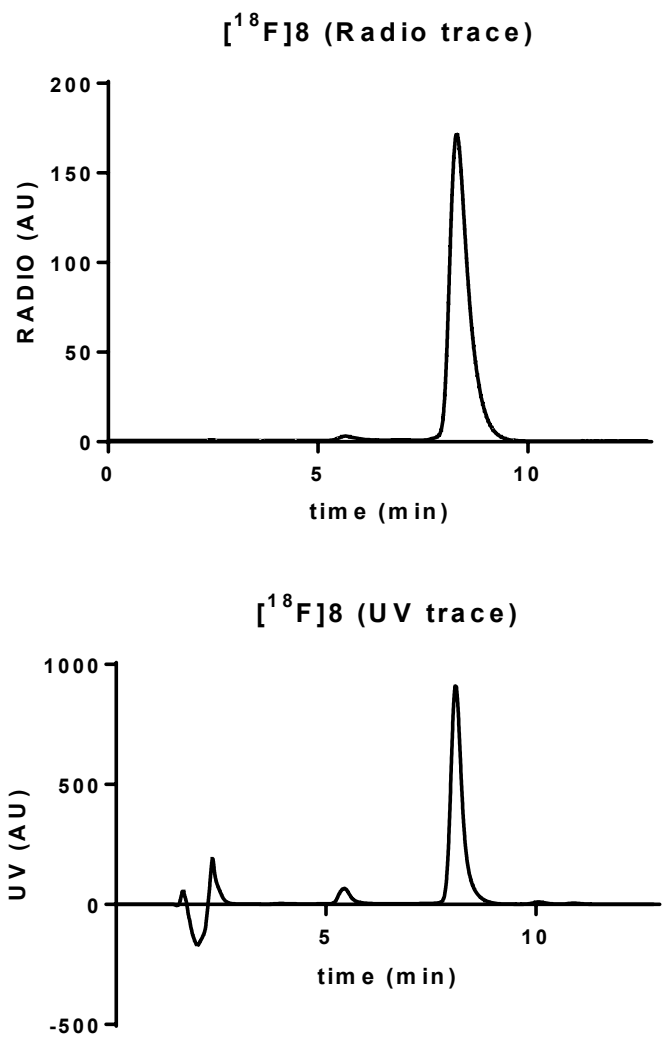


Figure S 18 - QC analysis of [<sup>18</sup>F]8.

1. Liu ZB, Pourghiasian M, Benard F, Pan JH, Lin KS, Perrin DM. Preclinical Evaluation of a High-Affinity F-18-Trifluoroborate Octreotate Derivative for Somatostatin Receptor Imaging. *Journal of Nuclear Medicine*. 2014;55:1499-1505.
2. Pourghiasian M, Liu ZB, Pan JH, et al. F-18-AmBF3-MJ9: A novel radiofluorinated bombesin derivative for prostate cancer imaging. *Bioorganic & Medicinal Chemistry*. 2015;23:1500-1506.
3. Maresca KP, Hillier SM, Femia FJ, et al. A Series of Halogenated Heterodimeric Inhibitors of Prostate Specific Membrane Antigen (PSMA) as Radiolabeled Probes for Targeting Prostate Cancer. *Journal of Medicinal Chemistry*. 2009;52:347-357.
4. Horiuchi T, Chiba J, Uoto K, Soga T. Discovery of novel thieno[2,3-d]pyrimidin-4-yl hydrazone-based inhibitors of Cyclin D1-CDK4: Synthesis, biological evaluation, and structure-activity relationships. *Bioorganic & Medicinal Chemistry Letters*. 2009;19:305-308.
5. Zhou Z, Fahrni CJ. A fluorogenic probe for the copper(I)-catalyzed azide-alkyne ligation reaction: Modulation of the fluorescence emission via (3)(n,pi\*)-(1)(pi,pi\*) inversion. *Journal of the American Chemical Society*. 2004;126:8862-8863.
6. Bouvet V, Wuest M, Jans H-S, et al. Automated synthesis of [18F]DCFPyL via direct radiofluorination and validation in preclinical prostate cancer models. *EJNMMI Research*. 2016;6:40.
7. Mukherjee S, van der Donk WA. Mechanistic Studies on the Substrate-Tolerant Lanthipeptide Synthetase ProcM. *Journal of the American Chemical Society*. 2014;136:10450-10459.
8. Benešová M, Schäfer M, Bauder-Wüst U, et al. Preclinical Evaluation of a Tailor-Made DOTA-Conjugated PSMA Inhibitor with Optimized Linker Moiety for Imaging and Endoradiotherapy of Prostate Cancer. *Journal of Nuclear Medicine*. 2015;56:914-920.